Stage-dependent regulation of intracellular calcium by spontaneous activity in developing brainstem

Hirofumi Watari

A dissertation

submitted in partial fulfillment of the

requirements for the degree of

Doctor of Philosophy

University of Washington

2013

Reading Committee:

Martha Bosma, Chair

William Moody

Horacio de la Iglesia

Program Authorized to Offer Degree:

Neurobiology & Behavior

University of Washington

Abstract

Stage-dependent regulation of intracellular calcium by spontaneous activity in developing brainstem

Hirofumi Watari

Chair of the Supervisory Committee:
Associate Professor Martha M. Bosma
Department of Biology

Spontaneous activity supports developmental processes in many brain regions during embryogenesis, and the spatial extent and frequency of the spontaneous activity are tightly regulated by stage. In the developing mouse hindbrain, spontaneous activity propagates widely and the waves can cover the entire hindbrain at E11.5. The activity then retracts to waves that are spatially restricted to the rostral midline at E13.5, before disappearing altogether by E15.5. However, the mechanism of retraction is unknown. We studied passive membrane properties of cells that are spatiotemporally relevant to the pattern of retraction in mouse embryonic hindbrain using whole-cell patch clamp and Ca_i^{2+} imaging techniques. We find that membrane excitability progressively decreases due to hyperpolarization of resting membrane potential and increased resting conductance density between E11.5-E15.5, in a spatiotemporal pattern correlated with

the retraction sequence. Retraction can be acutely reversed by membrane depolarization at E15.5, and the induced events propagate similarly to spontaneous activity at earlier stages, though without involving gap junctional coupling. Manipulation of $[K^+]_o$ or $[Cl^-]_o$ reveals that membrane potential follows E_K more closely than E_{Cl}, suggesting a dominant role for K^+ conductance in the membrane hyperpolarization. Reducing membrane excitability by hyperpolarization of the resting membrane potential and increasing resting conductance are effective mechanisms to desynchronize spontaneous activity in a spatiotemporal manner, while allowing information processing to occur at the synaptic and cellular level.

Between embryonic days (E) 11.5 and E13.5, spontaneous events propagate across the mouse brainstem as waves, each of which is driven by membrane depolarization, leading to calcium influx. Most calcium events rise from and return to a defined baseline. However, at E12.5, events rapidly burst with $[Ca^{2+}]_i$ staying close to peak value, well above baseline, for up to tens of minutes; we termed this Bash Bursts (Bash-B). Here, we investigate the mechanism of this unusual activity using calcium imaging and electrophysiology. Bash-B is triggered by an event originating at the midline of the rostral hindbrain, and is usually the result of that event propagating along a defined circular path. The looping circuit can either encompass both the midbrain and hindbrain, or remain in the hindbrain only, and the type of loop determines the duration of a single lap time, 5 or 3 s, respectively. Bash-B is supported by high membrane excitability of midline cells and is regulated by persistent inward “window current” at rest, contributing to spontaneous activity. The looping propagation pattern that underlies Bash-B is inhibited by flupirtine and APV, acting on unknown targets. A looping circuit is

an effective mechanism for increasing $[Ca^{2+}]_i$ at regular intervals. Bash-B disappears by E13.5 via alteration of the looping circuit, making Bash-B a short phenomenon. The resulting sustained $[Ca^{2+}]_i$ may influence development of raphe serotonergic and ventral tegmental dopaminergic neurons by modulating gene expression.

TABLE OF CONTENTS

Page

LIST OF FIGURES iv

Chapter 1: General Introduction 1

Anatomy of the brainstem 2

Spontaneous activity propagates synchronously at E11.5 3

Spontaneous activity causes influx of calcium 4

Specific Aims 5

Chapter 2: Hyperpolarization of resting membrane potential causes retraction of spontaneous intracellular calcium transients during mouse embryonic circuit development 7

Introduction 7

Methods 8

Animals *8*

Calcium Imaging *9*

Electrophysiology *9*

Results 11

Spontaneous activity retracts and disappears between E11.5-E15.5 *11*

Membrane hyperpolarizes from E11.5-E15.5 *11*

Resting conductance density increases from E11.5-E15.5 *14*

Retraction can be reversed by membrane depolarization at E15.5 *15*

Induced events propagate similarly to spontaneous activity *18*

Discussion 20

Possible mechanism of membrane hyperpolarization *22*

Possible role for spontaneous activity retraction *24*

Chapter 3: Looping circuit: a novel mechanism for prolonged spontaneous intracellular calcium increases in developing embryonic mouse brainstem 27

Introduction 27

Methods 29

Animals and Dissections *29*

Calcium imaging *29*

Electrophysiology *30*

Results 31

Sustained intracellular calcium in midline cells of rostral brainstem at E12.5 *31*

Directionality is predictable for hindbrain-only loops *37*

Membrane excitability peaks in InZ cells at E12.5 *39*

Midbrain cells are less excitable than hindbrain cells at E12.5 *42*

Bash-B ceases by E13.5, can it be rescued? *45*

Infinite loop? Will it ever end? *48*

Looping propagation is inhibited by flupirtine and APV *51*

Discussion 53

A looping circuit is a key underlying mechanism of Bash-B *53*

Window current may contribute to spontaneous activity but is not directly causative of loops *54*

Refractory period dictates the flow and directionality of calcium waves *56*

Variants of the looping circuit provide the means to vary frequency of calcium input *56*

Midbrain influences the fate of event propagation *57*

Neurotransmitter systems that support spontaneous activity changes across stages *58*

Chapter 4: General Conclusions and Future Directions 60

References 63

LIST OF FIGURES

Figure Number		Pages
1.1	Dopaminergic and serotonergic neurons develop in brainstem	3
2.1	Spontaneous activity retracts and disappears between E11.5-E15.5	12
2.2	Membrane potential hyperpolarizes from E11.5-E15.5 with changes in resting conductance density	13
2.3	Cessation of events can be reversed by membrane depolarization at E15.5	17
2.4	Evoked events propagate independently of gap junction coupling in E15.5	19
2.5	Pattern of hyperpolarization matches pattern of retraction temporally and spatially	22
3.1	A sustained increase in $[Ca^{2+}]_i$ in the midline of the hindbrain at E12.5	33
3.2	Bash-B is a result of a looping calcium event at E12.5	35
3.3	Midbrain-hindbrain loops underlie Bash-B and have a characteristic 5-s lap time	36
3.4	Variations of loops that underlie Bash-B	38
3.5	Window current peaks at E12.5 and makes lnZ cells more excitable	41
3.6	Midbrain cells are less excitable than hindbrain cells at E12.5, expressing less inward and more outward current densities	44
3.7	Calcium events do not loop at E13.5	47
3.8	Four independent mechanisms that underlie the end of a looping pattern	50
3.9	Bash-B is selectively inhibited by flupirtine and APV	52

Acknowledgments

Graduate school was a long journey. I worked on countless thesis projects. I failed many times. The taste of failure was bitter and discouraging at times, but it taught me many lessons. It was also what kept me going. After too many failures, when the door was almost closed, it made me realize how much I really wanted to do this. Looking back, this was hardly a lonesome journey. I worked with people who have influenced me, taught me, and molded me into the person that I am today. They helped me become a better neuroscientist. I have many people to acknowledge and say thanks to.

I'd like to thank Marti Bosma, who gave me a chance to continue a career in neuroscience. Marti was my supporter, my mentor, my second mom, and, at times, a tough boss. Marti provided me an environment that allowed me to focus on experiments, and repeatedly demonstrated trust that I could do this.

I'd like to thank the members of the Bosmanians for putting up with me daily and for their support and encouragements: Mark Shi, Bess Navarrete, Kyle Muir, Lucy Liu, James Liu, Veronica Rodriguez, Amanda Tose, Bethanny Danskin, Ashley Lin, Jesse Miles, Helen Jones and Christy Kang. Special thanks to the three research scientists, Mark, Bess, and Amanda. Without them I could not have done this. They were my colleagues, who spent countless hours in the lab working to solve problems with me. They were also my friends, who hung out with me, fed me, and generally made me feel happy to come to work every day.

I'd like to thank my committee members for supervising my progress: Bill Moody, Horacio de la Iglesia and Peter Detwiler. I'd also like to extend my thanks to Sandy Bajjalieh and David Perkel for serving on my committee in the early years.

I'd like to thank Bill Catterall, Todd Scheuer, and Jane Sullivan for training me early in graduate school. The skills that I gained in electrophysiology and computer programing were essential to my dissertation work. My experience in their labs helped me lay a foundation to become a better scientist.

Teamwork has been an integral part of my work. I'd like to thank many colleagues who collaborated with me: Alex Few, Xin Jiang, Jonathan Ting, Kara Pratt, Kyle Muir, Bess Navarrete and Amanda Tose. Special thanks to Amanda Tose, who collaborated with me on many of the key experiments that appears in this dissertation.

I'd like to thank Bill Moody and his lab, especially Curtis Easton for discussing science with me and Wanda Moats for her assistance.

Special thanks to Joseph Bosma-Moody for being my enthusiastic assistant in the lab and for being a strong ally when I needed something from Marti.

I'd like to thank Graduate Program in Neurobiology & Behavior, especially Ann Wilkinson and Lucia Wisdom for helping me with administrative stuff over the years. I'd like to thank the directors, Mike Shadlen, Tom Reh, Sheri Mizumori, Mark Bothwell, Eliot Brenowitz, Jane Sullivan and David Perkel for their advice and support throughout my graduate career.

I'd like to thank the Undergraduate Neurobiology Program. That's where my roots are, and during graduate school I had the privilege to give back to the program as

a TA. Thanks to Bill Moody and Michael Kennedy for giving me outstanding opportunities to teach.

Special thanks to Don Born for mentoring me as an undergraduate student. He was one of the first individuals who introduced scientific research to me, and I have since come to realize the importance of his teachings, which helped me throughout graduate school. Thanks, Dr. Born!

I have made great friends in Seattle over the years. Thanks to coaches Dan Kronmal, Drew Takac, Steph Bucks and my teammates for giving me a place to play softball for many years. Thanks to Seth Maristuen and the members of Off Constantly for making dodgeball one of my favorite sports. To my friends who are close to my heart: Amanda Tose, Marina Kuznetsova, Scott Votaw, Steph Bucks, Bess Navarrete, Joy Sebe, Nolan Roquet and Robin Harris. Words are not enough to tell them how much I value them in my life. The last several years have been a great opportunity for personal growth because of the positive influences I have gotten from them.

The economy went into recession while I was in graduate school. The budget cuts hit labs everywhere hard. I'd like to thank Jonathan Ting, a visionary, and Bryan White, an outreach superstar, for working with me to promote public awareness of the brain research as an effort to build support for our future through public education and community outreach. I am happy to see that members of Neurobiology & Behavior Community Outreach are continuing in this effort both locally and globally. Special thanks to Eric Chudler for mentoring us over the years.

I’d like to give special thanks to Mr. Natsuyoshi Toyoda and his staff at Toyoda Sushi. They have seen me go through ups and downs, yet have always cheered me up with their friendliness and a dish of my favorite sushi.

Lastly, I’d like to thank my parents, Kazuya and Junko, brothers Masa and Taka, grandmother Tamiko, and my extended family Emiko and Katherine for patiently supporting me and believing in me.

Chapter 1: General Introduction

Proper development of the nervous system is critical for the normal physiological function and behavior of an animal. Robust growth occurs during embryogenesis, when cells proliferate, differentiate, migrate, extend processes, and form synapses on correct targets. Previously, these processes were thought to be mediated by preprogrammed genetic sequences, but current research suggests that cell activity also plays an important role (Flavell & Greenberg, 2008). This activity manifests as propagating waves of spontaneous electrical activity, which trigger calcium influx. The resulting increase in intracellular calcium ($[Ca^{2+}]_i$) is thought to be involved in the regulation of many cellular processes including gene expression (Moody & Bosma, 2005). Spontaneous activity occurs in many regions of the developing nervous system including the retina (Meister *et al.*, 1991), hippocampus (Garaschuk *et al.*, 1998), spinal cord (O'Donovan *et al.*, 1998), cortex (Corlew *et al.*, 2004) and brainstem (Gust *et al.*, 2003; Hunt *et al.*, 2005; Rockhill *et al.*, 2009).

Spontaneous activity occurs well before functional behaviors appear. For example, retinal spontaneous waves occur days before the animal can see (Wong, 1999). What is the role of activity that results in no behavioral outcome? Experimental alterations of this activity disrupts correct wiring of neuronal circuit formation later in development (Shatz, 1996). Retinal waves are one of the best characterized examples of spontaneous activity and its study provides hints as to how spontaneous activity may influence development in other brain regions. However, the role of spontaneous activity is still not well characterized in the developing brainstem. This dearth of information motivates my dissertation.

Anatomy of the brainstem

The brainstem forms from a part of the neural tube, in the partially closed dorsal end surrounding the fourth ventricle. The brainstem is derived from the metencephalon and mesencephalon, which later become the midbrain and hindbrain, respectively. The midbrain and hindbrain are separated by the midbrain-hindbrain organizer, or isthmus. The isthmus secretes transcription factors and growth factors, including FGF8 (Crossley *et al.*, 1996), which define the rostrocaudal axis of the brainstem. The midbrain is separated into the tegmentum ventrally and tectum dorsally, which display an arcuate segmentation of transcription factors (Sanders *et al.*, 2002). Dopaminergic neurons develop within the tegmentum starting at around E10.5 and continuing for several days in mice (Fenstermaker *et al.*, 2010). The hindbrain is a structure that is in between the midbrain and spinal cord, and it later becomes the pons, medulla and cerebellum. The hindbrain is segmented into rhombomeres earlier in development. Gene expression occurs independently in each segment, promoting differential development along the rostrocaudal axis of the hindbrain. A consequence of this segmentation is found in the anatomical location of serotonergic neurons, which appear first rostrally in former rhombomere (r) 1-r3, then caudally in r5-r7 (Bosma, 2010). These two clusters of serotonergic neurons are separated by r4, where serotonergic neurons are absent (Fig. 1.1). From E10.5 to E15.5, removing the mesenchyme from the hindbrain allows the tissue to lay flat in an open-book configuration (Gust *et al.*, 2003). This configuration leaves neural circuits undamaged and we can efficiently image changes in $[Ca^{2+}]_i$ because the wide surface of the hindbrain lays flat within the same plane of focus. The

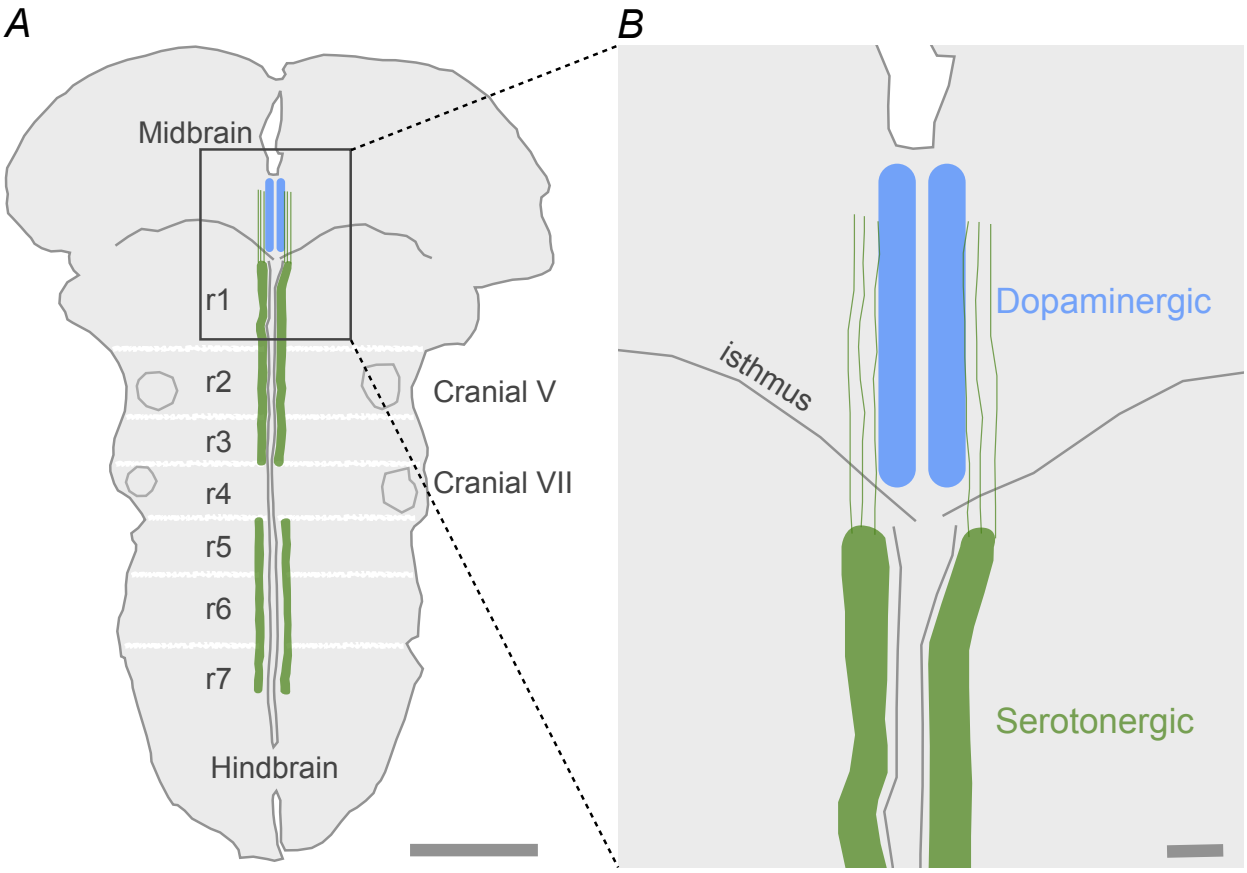

Figure 1.1. Dopaminergic and serotonergic neurons develop in brainstem
A, Brainstem in open-book configuration at E12.5. Rhombomeres (r) in the hindbrain disappear by E11.5, but former r1-r7 are reproduced on the diagram as a reference. Cranial V and VII are found laterally in r2 and r4, respectively. Dopaminergic neurons (blue) grow in the midbrain tegmentum along the midline axis. Serotonergic neurons (green) develop first in r1-r3, then in r5-r7. Scale: 1 mm. The squared region is scaled up in panel B. B, Dopaminergic and serotonergic neurons along the midline at the midbrain-hindbrain organizer, isthmus. A group of dopaminergic neurons (blue) are found in the midbrain tegmentum. The cell bodies of serotonergic neurons (green) are found along the midline axis of the hindbrain. Serotonergic neurons extend axons across the isthmic border, into the midbrain tegmentum where dopaminergic neurons grow. Scale: 100 μm.

rhombomeres disappear by E11.5 in mice, exactly when the propagation pattern of spontaneous activity switches from being asynchronous to synchronous (see below).

Spontaneous activity propagates synchronously at E11.5

Coinciding with the timing of rhombomere disappearance, at E11.5, spontaneous activity propagates synchronously across the entire hindbrain (Gust *et al.*, 2003). The spontaneous activity has a defined origin, called the initiation zone (InZ) (Moruzzi *et al.*,

2009), located on the midline of r2. Nearly 85% of spontaneous events originate from the InZ (Hunt *et al.*, 2006*b*). Furthermore, nearly 80% of neurons at the InZ are serotonergic, and a blockade of $5HT_{2AC}$ receptors with ketanserin inhibits spontaneous activity (Hunt *et al.*, 2005). This evidence suggests that serotonergic neurons are the candidate drivers of spontaneous activity in the embryonic mouse hindbrain.

Spontaneous activity causes influx of calcium

Spontaneous activity is driven by membrane depolarization. The midline cells of the hindbrain have a lower conductance compared to follower lateral cells (Moruzzi *et al.*, 2009). Midline cells also express Ca_V3 channels mediating T-type Ca^{2+} current. Spontaneous membrane depolarization causes calcium influx, and the resulting increases in $[Ca^{2+}]_i$ can be detected by cytoplasmic calcium indicators such as Fluo-4 and Fluo-8 in calcium imaging. Calcium imaging data reveals that $[Ca^{2+}]_i$ increases first at the InZ (Hunt *et al.*, 2006*b*). This is followed by $[Ca^{2+}]_i$ increases in neighboring cells, as propagating waves spread across the entire hindbrain at E11.5.

Propagation pattern changes, and eventually disappears, across stages of hindbrain maturation

Whereas the $[Ca^{2+}]_i$ increase spreads from the InZ to the entire surface of the hindbrain at E11.5, the propagation pattern changes dramatically across stages (Hunt *et al.*, 2006*b*). At E12.5, the extent of the spread retracts from lateral cells and propagation is restricted to the midline of the hindbrain. The propagating waves can extend into the midbrain tegmentum, where events can sporadically branch laterally

(dorsally) along the isthmic border (Rockhill *et al.*, 2009). At E13.5, the propagation is restricted to the midline and cannot extend more caudally than r5. By E14.5, the spontaneous activity vanishes from the hindbrain (Hunt *et al.*, 2006*b*). The mechanism by which activity retracts spatiotemporally is unknown. In addition, between E11.5-E13.5, the frequency of events is altered as well. The frequency peaks at E11.5 where events occur at 3/min (Hunt *et al.*, 2005; 2006*b*). Whereas calcium events at most stages elevate calcium from a defined baseline, at E12.5, events can occur at such a high frequency that events summate. This causes $[Ca^{2+}]_i$ to remain above baseline levels for a prolonged period of time. This summation phenomenon disappears by E13.5, when the frequency of events decreases to 2/min (Hunt *et al.*, 2006*b*). The mechanism behind the dramatic and short-lived high frequency calcium events at E12.5 is unknown.

Specific Aims

I directed my research to answer two specific questions regarding spontaneous activity in the developing embryonic mouse brainstem. First, what is the mechanism that drives spatiotemporal retraction and eventual disappearance of spontaneous activity in the hindbrain? Secondly, what is the mechanism that produces episodes of high frequency calcium events in the rostral brainstem at E12.5?

Specific Aim I: mechanism of retraction

Retraction of spontaneous activity is a process that occurs both in space and time; each stage between E11.5 and E13.5 has its own unique and subsequently

reduced spread of activity (Hunt *et al.*, 2006*b*). We hypothesized that retraction is a result of changes to cell membrane properties, which occur first laterally, and then medially towards the InZ. To test this, we performed patch clamp recordings from E10.5-E15.5 at locations that are relevant to the spatial pattern of retraction. These positions include: lateral r2, where retraction is first observed at E12.5; midline r5, where retraction occurs at E13.5; and midline r2 (InZ), where retraction occurs at E14.5. This study is detailed in Chapter 2.

Specific Aim II: mechanism of prolonged above-baseline $[Ca^{2+}]_i$ events

The prolonged above-baseline $[Ca^{2+}]_i$ events occur most prevalently at E12.5. This novel phenomenon, termed Bash Bursts (Bash-B), was previously uncharacterized. Thus the goal of this aim is divided into two parts: first, we focused on a precise description of Bash-B; second, we sought to identify the mechanism underlying the unusual propagation patterns. We employed calcium imaging to study propagation patterns of events, electrophysiological recordings to study membrane properties that support Bash-B, and pharmacological agents to attempt to modulate Bash-B. The study is detailed in Chapter 3.

Chapter 2: Hyperpolarization of resting membrane potential causes retraction of spontaneous intracellular calcium transients during mouse embryonic circuit development

Introduction

Spontaneous electrical activity supports activity-dependent neuronal circuit formation (Moody & Bosma, 2005) by varying $[Ca^{2+}]_i$ in a temporally-specific manner during embryogenesis, affecting gene expression and resultant phenotypes (Spitzer, 2006). Spontaneous activity is a conserved phenomenon among developing vertebrates and has been shown to occur in rat (Garaschuk *et al.*, 2000), mouse (Corlew *et al.*, 2004; Hunt *et al.*, 2005) and chick (O'Donovan *et al.*, 1998; Hughes *et al.*, 2009; Wang *et al.*, 2009) embryonic and neonatal nervous systems. Spontaneous activity occurs in many regions of the developing nervous system including neocortex (Garaschuk *et al.*, 2000; Corlew *et al.*, 2004), retina (Meister *et al.*, 1991), spinal cord (O'Donovan *et al.*, 1998), midbrain (Rockhill *et al.*, 2009), and hindbrain (Hunt *et al.*, 2005).

The spatial extent and frequency of spontaneous activity appear to be regulated precisely in a temporal fashion (Hunt *et al.*, 2006*b*; Conhaim *et al.*, 2011), most likely to regulate sequences of gene expression. In the mouse hindbrain, the midline and lateral cells experience repetitive events involving a rise in $[Ca^{2+}]_i$ at E11.5 (Gust *et al.*, 2003) driven by spontaneous membrane depolarization (Moruzzi *et al.*, 2009), and spontaneous activity can spread to cover the entire hindbrain (Hunt *et al.*, 2006*b*). However, this coverage area shrinks during development as the spread of spontaneous

activity retracts, first from lateral regions at E12.5, then, between E13.5-E14.5, towards the initiation zone (InZ), a defined origin at the midline of former rhombomere (r)2 (Moruzzi *et al.*, 2009). By E13.5, the frequency of spontaneous activity decreases, and the spontaneous activity disappears altogether from the hindbrain by E14.5 (Hunt *et al.*, 2006*b*; Bosma, 2010).

Because each spontaneous depolarizing event causes an influx of calcium (Moruzzi *et al.*, 2009), which can modulate cellular processes including gene expression, the timing and consequence of spontaneous activity retraction and ultimate disappearance likely has an impact on neuronal circuit formation during embryogenesis. How spontaneous activity retracts is still unknown. Here, we provide evidence that hyperpolarization of resting membrane potential and increased resting conductance may underlie the retraction of spontaneous activity in the embryonic mouse hindbrain. The resulting reduction in membrane excitability is an effective mechanism to desynchronize spontaneous activity in a spatiotemporal manner, while allowing information processing to occur at the synaptic and cellular level.

Methods

Animals

Timed-pregnant Swiss/Webster mice were either bred in the lab or purchased from Harlan Laboratories (Livermore, CA, USA). The animals were sacrificed by CO_2 followed by cervical dislocation. Care for animals and euthanasia procedures were approved by University of Washington Animal Care Committee (IACUC). Embryos at E10.5-E15.5 were kept in ACSF, containing (in mM): 119 NaCl, 2.5 KCl, 1.3 $MgCl_2$, 2.5

$CaCl_2$, 1 NaH_2PO_4, 26 $NaHCO_3$, 30 glucose, and bubbled in carbogen (95% O_2, 5% CO_2). For high $[K^+]_o$ experiments, an equivalent molar concentration of NaCl was replaced by KCl. We used 12-15 mM $[K^+]_o$ for these experiments. For low $[Cl^-]_o$ experiments, an equivalent molar concentration of NaCl was replaced by sodium gluconate. All external solutions have osmolarity of 316 ± 1 mosmol/L. Hindbrains were dissected as previously described (Moruzzi *et al.*, 2009). All experiments were done at approximately 23 ˚C.

Calcium Imaging

Hindbrains were removed and incubated in oxygenated ACSF for 15 min with the $[Ca^{2+}]_i$ indicators fluo-4 or fluo-8 and pluronic F-127. The change in fluorescence was measured in up to 48 regions of interest (ROIs) in the former r2 or r5 regions using MetaFluor (Universal Imaging/Molecular Devices, Downington, PA, USA), with an image capture rate of 1 Hz or 2.43 Hz. The perfusion rate of the oxygenated ACSF was maintained at 1 ± 0.3 mL/min during recording. Meclofenamic acid was from Sigma-Aldrich Co., St. Louis, MO, USA. Mefloquine was from Tocris Bioscience, Ellisville, MO, USA. The calcium imaging data were visualized and analyzed in ImageJ (National Institutes of Health, Bethesda, MD, USA) and Igor Pro 6 (Wavemetrics, Inc. Lake Oswego, OR, USA) with custom functions developed by Hirofumi Watari.

Electrophysiology

Whole-cell patch clamp recording was performed on cells from three hindbrain regions: at the midline in the former r2 where >90% of spontaneous activity events

originate (InZ); in lateral cells 200 μm from the midline of the InZ; and midline cells in the former r5, where events rarely initiate. Pipettes of resistance 2.5-5 MΩ approached from the ventricular side in the open-book configuration, as described previously (Moruzzi *et al.*, 2009). Internal solution contained (in mM): 100 K-gluconate, 15 KCl, 1 EGTA, 5 $MgCl_2$, 40 HEPES, 3 Na-ATP, 0.3 Na-GTP (adapted from Mooney *et al.*, 1996; Moruzzi *et al.*, 2009). pH was titrated to 7.25 by addition of NaOH. Osmolarity was adjusted to 328 ± 2 mosmol/L by addition of sucrose. For these solutions, E_K=-97.4 mV and E_{Cl}=-42.2 mV (Hille, 2001). The perfusion rate of the oxygenated ACSF was maintained at 1 ± 0.3 mL/min during recording. Data were acquired using Axopatch-1D or Axopatch 200B amplifier with pClamp 8 (Molecular Devices, LLC. Sunnyvale, CA, USA). Signals were low-pass Bessel filtered with cutoff frequencies of 2 or 5 kHz. Signals were digitized at 5-10 kHz. In the ramp voltage-clamp experiment, first the voltage was stepped from the holding potential of -60 mV to +80 mV for 150 ms to inactivate inward current response, then ramped from +80 mV to -100 mV at the rate of -233 mV/s. This rate is equivalent to the protocol used previously (Moruzzi *et al.*, 2009). The current clamp traces were decimated offline without smoothing by a factor of 10 to an equivalent of 500 Hz sampling frequency to reduce the baseline noise that was introduced due to oversampling; the decimation effectively reduced baseline noise without affecting the waveform of the events. Liquid junction potential of -6.3 mV caused by the perfusion of low $[Cl^-]_o$ ACSF was calculated in Clampex (Molecular Devices, LLC. Sunnyvale, CA, USA) and was corrected for offline. All analyses were done using Igor Pro 6 with custom functions developed by Hirofumi Watari.

Results

Spontaneous activity retracts and disappears between E11.5-E15.5

In the developing mouse embryonic hindbrain, spontaneous $[Ca^{2+}]_i$ transients are driven by spontaneous membrane depolarization (Moruzzi *et al.*, 2009), which opens $Ca_V3.3$ channels mediating T-type Ca^{2+} currents and causes a rise in $[Ca^{2+}]_i$ (Hughes *et al.*, 2009; Moruzzi *et al.*, 2009). Most Ca^{2+} events initiate in the midline of former r2 (the initiation zone, or InZ) at E11.5 (Fig. 2.1A, 1.6 s) and occur with a frequency of 3.2 ± 0.2/ min (Hunt *et al.*, 2006*b*). These events propagate rostrally and caudally along the midline of the hindbrain (Figs. 2.1B, D, top left; Fig. 2.1C, left, dark red), and, with lower intensity and frequency, into the lateral regions (Hunt *et al.*, 2005) (Figs. 2.1B, D, bottom left; Fig. 2.1C, left, light red). The propagation requires both $5\text{-}HT_{2A,C}$ receptor activation and gap junctional coupling, as judged by the block of activity by ketanserin, spiperone and gap junction blockers (Hunt *et al.*, 2005; 2006*a*). Over the course of development, at E13.5, spontaneous activity retracts towards the InZ (Figs. 2.1B, C, D, middle; Hunt *et al.*, 2006*b*). Waves in the lateral regions disappear (Fig. 2.1D, bottom middle) and do not propagate as caudally as it does in the midline of E11.5 (Fig. 2.1D, top middle). All events are extinguished at E15.5 (Figs. 2.1 B, C, D, right).

Membrane hyperpolarizes from E11.5-E15.5

We asked whether retraction is caused by spatially regulated changes in intrinsic membrane properties. We performed whole-cell patch clamp on cells from three sites that are spatially and temporally relevant to the pattern of retraction: the InZ (r2 midline) where most events originate and where events persist into late stages (Fig. 2.2A, grey);

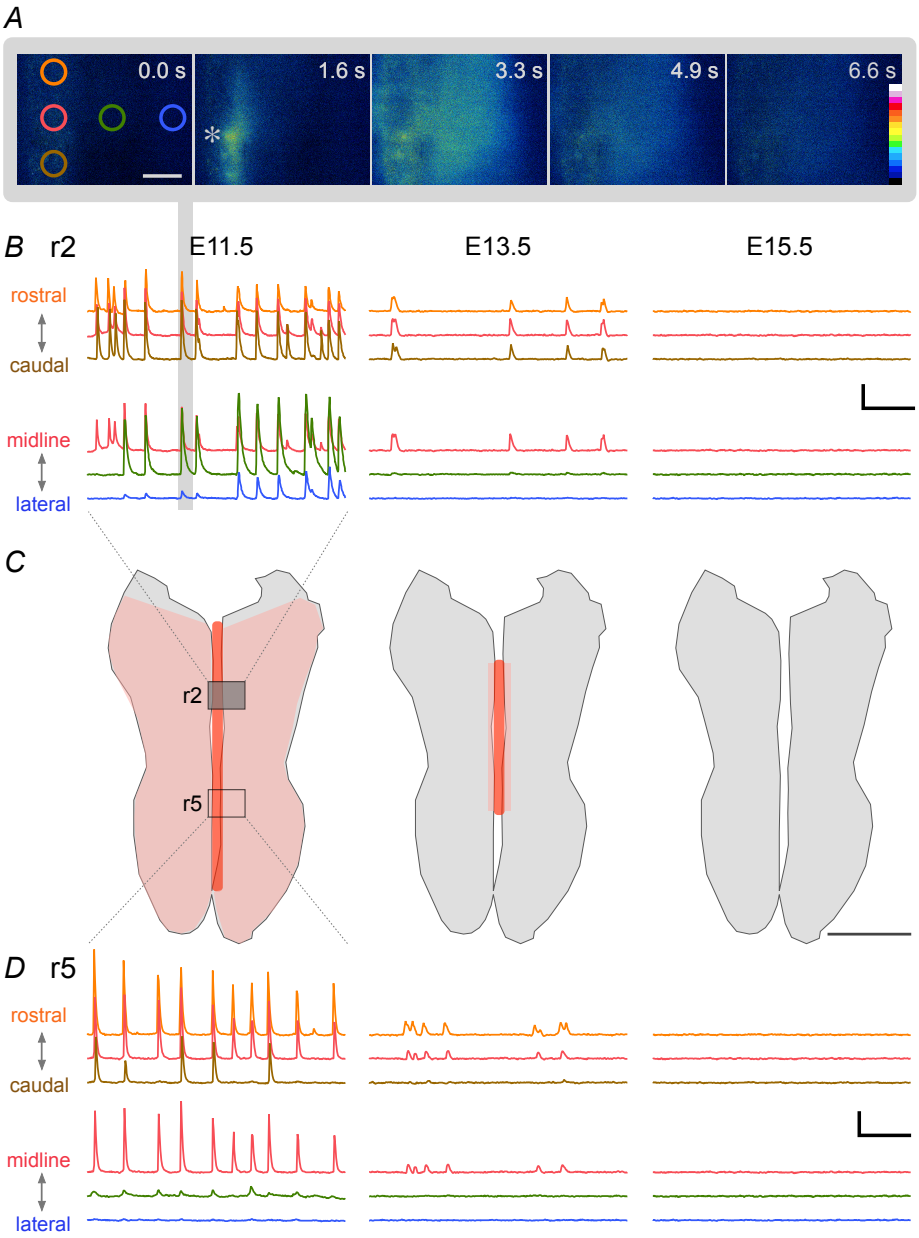

Figure 2.1. Spontaneous activity retracts and disappears between E11.5-E15.5
A, frames of images show initiation and propagation of an event at E11.5. The images were pseudocolored to show a gradient of intensities in the fluorescence (white, high intensity; black, low intensity). The colored circles indicate regions of interests (ROIs, at 0.0 s) positioned along the midline (orange, red, brown) and mediolaterally (red, green, blue) within former rhombomere (r)2. Initiation of an event starts as an increase in fluorescence at 1.6 s (InZ, indicated by *). The event then spreads along the midline axis (1.6, 3.3 and 4.9 s) and then laterally (3.3 and 4.9 s). Scale bar: 100 μm. B, Representative $[Ca^{2+}]_i$ traces recorded at E11.5 (left), E13.5 (middle) and E15.5 (right) in r2, showing rostrocaudal (top) and mediolateral (bottom) propagation. Traces are stacked and the color corresponds to the position of ROIs shown in A. The event from the images in A is marked with grey vertical bar. Scale bar (applies to all graphs): 5 ΔF/F, 1 min. C, Spread of spontaneous activity is greatest at E11.5 (left) where it can cover the entire surface of the hindbrain. Intensity of Ca^{2+} signal is greater at the midline (dark red) compared to the lateral regions (light red). The region of Ca^{2+} imaging shown in panels A and B is indicated by grey rectangle, marked “r2”. The region of Ca^{2+} imaging shown in panel D is indicated by open rectangle, marked “r5” (left). The propagation retracts laterally and medially at E13.5 (middle). Spontaneous activity disappears by E15.5 (right). Some parts of the figure are adapted and modified from Hunt *et al.*, 2006*b*. Scale bar: 1 mm. D, Representative $[Ca^{2+}]_i$ traces recorded at E11.5 (left), E13.5 (middle) and E15.5 (right) in r5, marked by the open rectangle in panel C, showing rostrocaudal (top) and mediolateral (bottom) propagation. Traces are stacked and the color corresponds to the position of ROIs shown in A. Scale bar (applies to all graphs): 5 ΔF/F, 1 min.

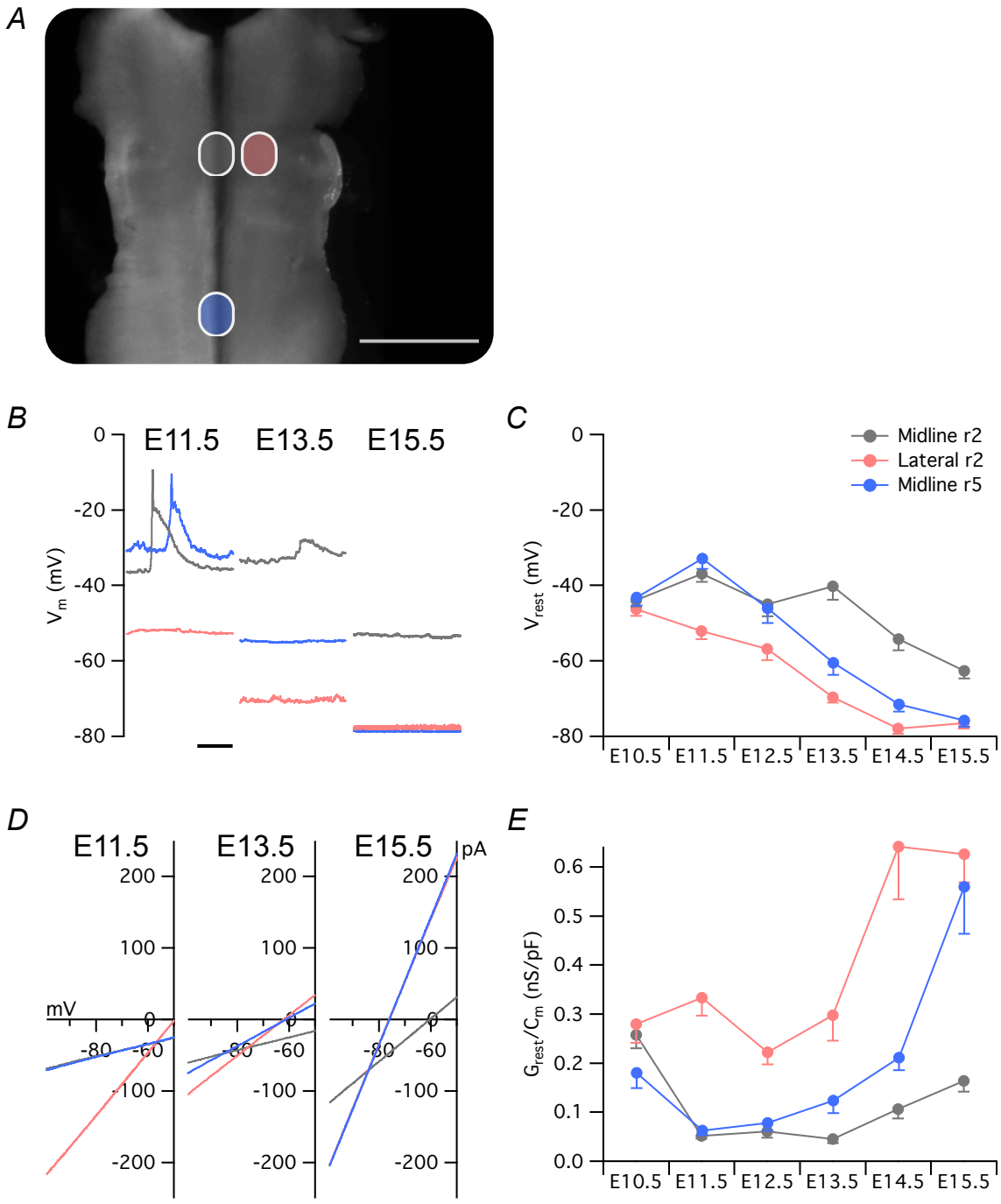

Figure 2.2. Membrane potential hyperpolarizes from E11.5-E15.5 with changes in resting conductance density

A, Light microscope image of the hindbrain used in electrophysiology experiments. Whole-cell patch clamp was performed on cells in three colored regions: midline r2 (grey, InZ), lateral r2 (red), midline r5 (blue). Scale bar: 1 mm. B, Representative membrane potential (V_m) is shown for cells recorded in current clamp at three stages: E11.5 (left), E13.5 (middle) and E15.5 (right). Each colored trace represents V_m recorded from a cell in the regions as shown in Figure 2.2A. Scale bar: 1 s. C, Mean resting membrane potential at each stage from E10.5-E15.5. D, Averaged current-voltage (IV) relations after delivering a voltage ramp protocol. At E11.5, the resultant currents from averaged midline r2 and midline r5 cells completely overlap; at E15.5, the currents from midline r5 and lateral r2 overlap. Note the progressive hyperpolarization of the zero-current potential, corresponding to the shift in V_{rest}. E, Mean resting conductance measured as a slope of the IV relations in D, normalized for membrane capacitance. In panels B and D, the negative bar represents SEM and n>13 at each stage and location. In all panels, color of the trace corresponds to regions defined in A.

lateral cells 200 µm from the InZ, where events retract first (Fig. 2.2A, red); and midline cells in the former r5, where events rarely initiate but where events propagate until E13.5 (Hunt *et al.*, 2006*b*) (Fig. 2.2A, blue).

Current clamp recordings reveal that cells at all three sites have equivalent resting membrane potentials at E10.5 (Fig. 2.2C). Then, the membrane hyperpolarizes progressively between E11.5-E15.5 (Fig. 2.2B, C). The hyperpolarization occurs first in lateral cells (red traces; -52.1 ± 2.1 mV at E11.5, n=14 *vs.* -76.4 ± 1.4 mV at E15.5, n=20; ***p<0.001). Subsequently, midline cells in the caudal sites hyperpolarize and have the largest change of up to 50 mV (blue traces; -32.8 ± 2.7 mV at E11.5, n=19 *vs.* -75.8 ± 1.7 mV at E15.5, n=15; ***p<0.001). The cells of the InZ remain depolarized until E13.5. They then hyperpolarize, and to the least extent (grey traces; -40.2 ± 3.6 mV at E13.5, n=15 *vs.* -62.6 ± 2.0 mV at E15.5, n=15; **p<0.01). The pattern of hyperpolarization mirrors the spatial pattern of retraction of spontaneous activity (Hunt *et al.*, 2006*b*). We next investigated the mechanism of the hyperpolarization.

Resting conductance density increases from E11.5-E15.5

We have previously shown that lateral cells have a significantly higher resting conductance than midline cells at E11.5 (Moruzzi *et al.*, 2009), and our current data confirms this difference (Fig. 2.2D, E, red *vs.* grey traces at E11.5). We measured current-voltage (IV) relations using a voltage ramp protocol at E11.5, E13.5 and E15.5. The IV relation is linear between -90 mV and -60 mV, and the slope within this range is used to measure the conductance (Fig. 2.2D). To account for a possible change in cell size across stages, the conductance was normalized to membrane capacitance. In

lateral regions, where events propagate with lower $[Ca^{2+}]_i$ intensity, the resting conductance density is significantly higher than the midline cells at E11.5 (Fig. 2.2E; midline r2, grey, n=23 *vs.* lateral r2, red, n=13; ***p<0.001). The conductance density of the lateral cells nearly doubles between E13.5 and E14.5 (n=14 and n=15, respectively; **p<0.01) and it remains high at E15.5 (n=20; Fig. 2.2E, red). The midline cells in r5 display the most striking change over time (Fig. 2.2E, blue). The resting conductance density increases by nine-fold in just four days starting at E11.5 (E11.5, n=19 *vs.* E15.5, n=15; ***p<0.001), and matches the conductance density of the lateral cells by E15.5. Lastly, the cells in the InZ region show the most modest increase in conductance density of the three regions recorded (Fig. 2.2E, grey). The resting conductance density doubles between E13.5 and E14.5 (n=22 and n=32, respectively), the point in time after which the spontaneous activity ceases to be recorded. In summary, the resting conductance density increases by as much as nine-fold between E11.5 and E15.5, and the greatest change occurs at the sites away from the InZ. Both the resting membrane potential and resting conductance density in the InZ do not change between E11.5-E13.5, allowing initiation of spontaneous activity. The increase in resting conductance density indicates an increase in the density of resting channels, which may contribute to the hyperpolarization of the membrane potential reported above; the selectivity of these channels will be discussed below.

Retraction can be reversed by membrane depolarization at E15.5

Our data demonstrates that progressive hyperpolarization parallels retraction of spontaneous activity between E11.5-15.5. If this hyperpolarization causes retraction of

spontaneous activity, then acute membrane depolarization should induce events in regions that have undergone retraction. To test this, we increased $[K^+]_o$ to depolarize the membrane at E15.5. We performed whole-cell patch clamp in the midline cells of r5, where the greatest change in the resting membrane potential and resting conductance was observed between E11.5 and E15.5 (Fig. 2.2D, E). When $[K^+]_o$ was increased from 2.5 mM to 12-14 mM, the membrane potential of the r5 midline cells of previously quiescent E15.5 hindbrains depolarized from -69.8 ± 2.2 to -49 ± 1.2 mV (n=23, ***p<0.001), depolarizing the membrane so that the resultant resting membrane potential was closer to where it was at E12.5-E13.5, and events were induced (Fig. 2.3A). Frequency of events increased from zero to a mean of 1.8 ± 0.4 events/min (n=6; Fig. 2.3B). A significant change in membrane potential of 17.3 ± 2.4 mV occurred with acute application of 12 mM $[K^+]_o$ ACSF at E15.5 (n=8; Fig. 2.3C, closed circle). A corresponding change of 9.6 ± 2.3 mV was significantly smaller at E11.5 (n=8; Fig. 2.3C, open circle). These experiments show that the mechanisms that support propagation do not disappear during retraction, but are simply suppressed by hyperpolarization.

To test the role of Cl^- conductance in the hyperpolarization, we set E_{Cl} to more positive potentials, and asked if the membrane potential followed E_{Cl}. When $[Cl^-]_o$ was decreased from 129.1 to 39.1 mM (setting E_{Cl} from -41.9 to -11.4 mV), the membrane potential hyperpolarized by -14.6 ± 5.1 mV at E11.5 (n=6) and by -9.3 ± 1.6 mV at E15.5 (n=7) (Fig. 2.3D, E). At both stages, the membrane potential moved away from the E_{Cl} set by the low $[Cl^-]_o$ ACSF. Whereas the high $[K^+]_o$ ACSF moved the membrane potential towards both E_K and E_{Cl} (Fig. 2.3F, left), the low $[Cl^-]_o$ ACSF moved it towards

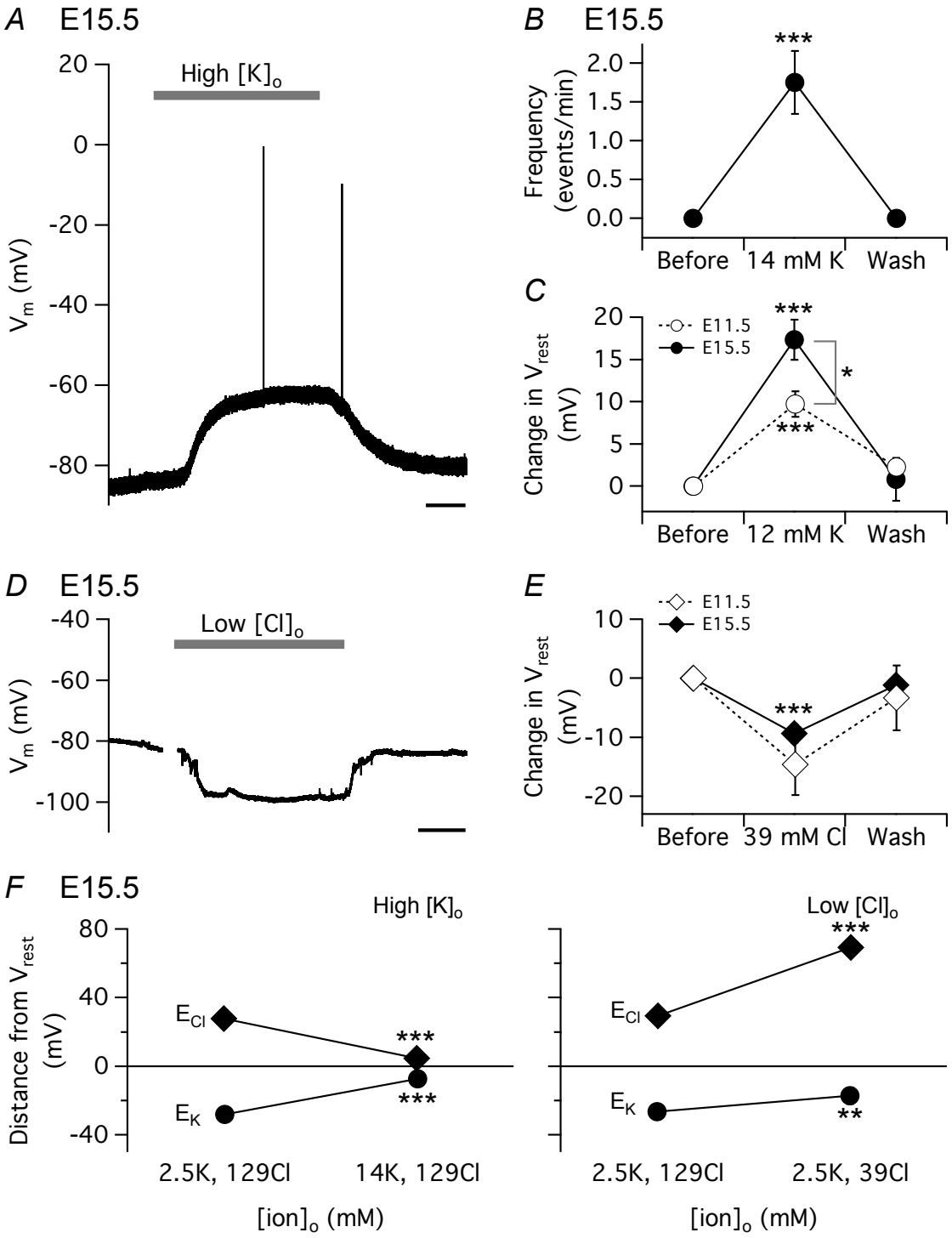

Figure 2.3. Cessation of events can be reversed by membrane depolarization at E15.5
A, Representative trace recorded from cells in midline r5 shows response to acute bath application of high $[K^+]_o$ ACSF. Scale bar: 2 min. B, Change in event frequency for cells in midline r5 during bath application and after washout of high $[K^+]_o$ ACSF. C, Change in V_{rest} recorded from cells in midline r5 during bath application and after washout of high $[K^+]_o$ ACSF. D, Representative trace recorded from cells in midline r5 shows hyperpolarizing response to acute bath application of low $[Cl^-]_o$ ACSF. Scale bar: 2 min. E, Change in V_{rest} recorded from cells in midline r5 during bath application and after washout of high $[Cl^-]_o$ ACSF. F, Distance in mV between the Nernst potentials [(E_K,(circles), E_{Cl} (diamonds)] and the V_{rest} before and during high $[K^+]_o$ ACSF (left) or low $[Cl^-]_o$ ACSF (right). The effect of liquid junction potential (-6.3 mV) caused by the application of low $[Cl^-]_o$ is corrected for in E and F but not in D. In panels B, C, E and F, the bars represent SEM.

E_K but away from E_{Cl} at E15.5 (Fig. 2.3F, right). These results suggest that the increased conductance may be due to an upregulation of K^+-permeable resting ion channels, while little Cl^- conductance is involved in the membrane hyperpolarization.

Serotonin (5-$HT_{2A,C}$) receptor activation is required for spontaneous activity at early stages indicated by the fact that ketanserin blocks events at E11.5 (Hunt *et al.*, 2005) and at E13.5 (Hunt *et al.*, 2006*a*). However, acute bath application of either 100-500 μM 5-HT (n=2) or 0.5-10 μM fluoxetine (n=2) failed to evoke events at E15.5 (data not shown), suggesting that a decrease in 5-HT receptor function alone does not cause retraction. In contrast, acute bath application of 2 μM AMPA, which is known to have a modulatory effect on frequency of spontaneous activity at E13.5 but not at E11.5 (Hunt *et al.*, 2006*a*), can evoke propagating events along the midline axis at E14.5-E15.5 (n=5, data not shown). These results suggests that the underlying mechanism of retraction is not dependent on loss of 5-HT receptor function, and the change in receptor phenotype that happens during retraction is supportive of propagation but not causative to the retraction itself.

Induced events propagate similarly to spontaneous activity

Our whole-cell patch clamp experiment showed that, at E15.5, the high $[K^+]_o$ ACSF induced events in individual cells in regions where spontaneous activity has already undergone retraction. We next investigated the spatial extent of the induced events using Ca^{2+} imaging. The events induced by high $[K^+]_o$ ACSF propagate along the midline axis at E15.5 (Fig. 2.4A, top), with restricted propagation laterally (Fig. 2.4A, bottom left), similarly to the way spontaneous activity propagates at earlier stages. The

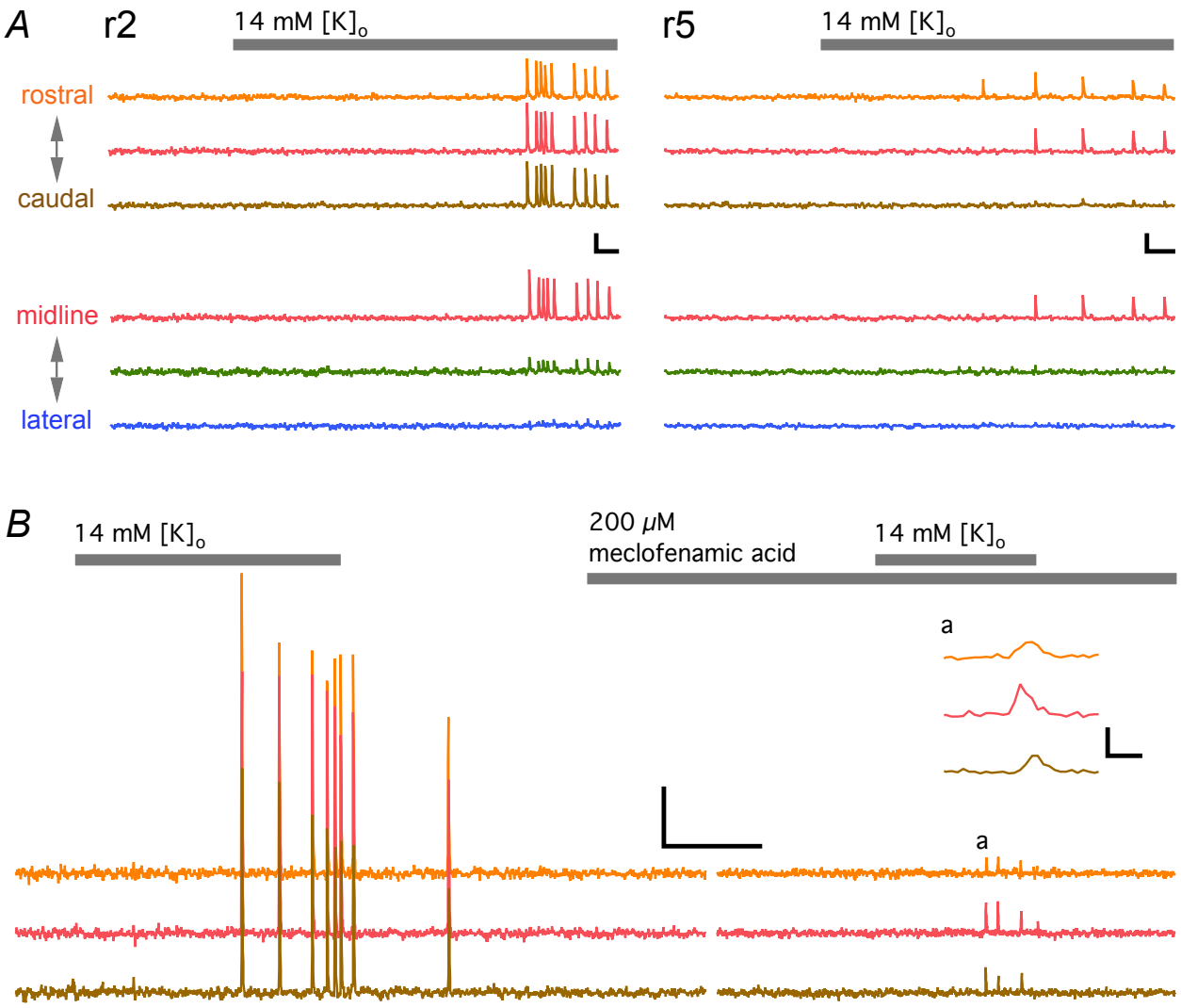

Figure 2.4. Evoked events propagate independently of gap junction coupling in E15.5
A, Representative ΔF/F fluorescence trace recorded at r2 (left) and r5 (right) show propagation of Ca^{2+} events along the midline axis (top) with restricted lateral spread (bottom left), caused by acute bath application of high $[K^+]_o$ ACSF. Separate experiments are shown for each region. The Ca^{2+} imaging in midline r5 (right) is recorded from the same location where electrophysiology was performed in Fig. 2.3. Scale bar (all graphs): 1 ΔF/F, 1 min. B, Representative ΔF/F fluorescence trace recorded at midline r2 show propagation of Ca^{2+} events along the midline caused by application of high $[K^+]_o$ ACSF in the absence and in the presence of meclofenamic acid at E15.5. Inset a, Representative ΔF/F fluorescence trace corresponding to label a in the main trace. Inactivity during drug application (14 min) is omitted from the trace. Scale bar: 2 ΔF/F, 5 min; 1 ΔF/F, 6 s (inset). The amplitudes of events look smaller during the second high $[K^+]_o$ probe because of photobleaching. In all panels, color of the traces indicate ROIs as shown in Fig. 2.1A.

induced events propagate through the midline of both r2 (Fig. 2.4A, left) and, notably, r5 (Fig. 2.4A, right), where propagation terminates caudally (Fig. 2.1D, top middle) and resting membrane hyperpolarizes most robustly (Fig. 2.2C, blue trace). This suggests

that mechanisms that support propagation may still be present in the quiescent E15.5 hindbrain. Propagation of spontaneous activity has been reported to involve gap junctional coupling in developing retina and neocortex (Roerig & Feller, 2000). Likewise, it is known that propagation requires gap junctional coupling at earlier stages in the hindbrain (Hunt *et al.*, 2006*a*). To test for a functional role of gap junction coupling at E15.5, we bath applied gap junction blockers and probed for events with high $[K^+]_o$ ACSF in the lnZ region. Whereas the events at E11.5 disappear with bath application of 200 μM meclofenamic acid (n=8, data not shown) or 100 μM mefloquine (n=5; also see Moruzzi *et al.*, 2009), the high $[K^+]_o$-induced events are still capable of propagating in the presence of these gap junction blockers at E15.5 (Fig. 2.4B, meclofenamic acid, 4/4; mefloquine, 5/6, data not shown). Events during the second high $[K^+]_o$ application have smaller amplitudes due to photobleaching (n=3 control experiments; data not shown). These results suggest that acute membrane depolarization can increase spatial extent of the induced events, and, at E15.5, such event propagation no longer requires gap junctional coupling.

Discussion

Activity-dependent gene expression has been proposed as a mechanism that is involved in neuronal circuit formation (Flavell & Greenberg, 2008). The key component to this hypothesis is the calcium influx, which can modulate many cellular processes including gene expression. Spontaneous activity during embryogenesis can support this function by regulating $[Ca^{2+}]_i$ both temporally and spatially, and may therefore orchestrate many developmental processes including proliferation, migration,

differentiation, transmitter phenotype, axonal guidance, synaptogenesis and ion channel expression (Moody & Bosma, 2005; Spitzer, 2006; Hanson *et al.*, 2008).

Several models describe spatiotemporal regulation of spontaneous activity (Butts *et al.*, 1999; Godfrey & Swindale, 2007; Hennig *et al.*, 2009). Spatiotemporal properties of retinal waves are influenced by a variable fraction of recruitable cells in the neighboring area, and the propagation stops when the fraction is small (Butts *et al.*, 1999). In this model, the recruitable cells are defined by an intrinsic refractory period, so each cell can theoretically switch from being recruitable to non-recruitable, and vice versa, within minutes if not seconds. Spontaneous activity retraction in the hindbrain, however, occurs over hours and days, so the recruitable cells must be defined by properties other than the refractory period.

We have found a novel mechanism of spontaneous activity retraction. Between E11.5-E15.5, the hindbrain cells exhibit a decrease in the membrane excitability measured by hyperpolarization of the resting membrane potential and increase in resting conductance (Fig. 2.2). At a stage before widespread waves of spontaneous activity occur, E10.5 (Gust *et al.*, 2003); unpublished observation), cells at all recorded sites have similar resting membrane potentials (Fig. 2.2C). Midline cells subsequently depolarize slightly, while lateral cells begin the process of gradual hyperpolarization. Then, the midline cells hyperpolarize, first at sites away from the InZ, then the InZ itself, defining the end of the window of spontaneous activity. The spatiotemporal pattern of this change (Fig. 2.5) matches the known spatiotemporal pattern of retraction (Hunt *et al.*, 2006*b*) (Fig. 2.1C). For example, the propagation of spontaneous activity terminates caudally in r4-r5 at E13.5 (Fig. 2.1D, top middle), and this Ca^{2+} imaging data

correlates well with the electrophysiology data that shows resting membrane hyperpolarization and increase in resting conductance density in r5 (Fig. 2.2C, E, blue traces). The retraction can be acutely reversed by membrane depolarization induced by application of high $[K^+]_o$ ACSF (Fig. 2.3, 2.4). Taken together, retraction is likely caused by the changes in the passive membrane properties of the cells.

Figure 2.5. Pattern of hyperpolarization matches pattern of retraction temporally and spatially
Spread of spontaneous activity is greatest at E11.5 where it covers the entire surface of the hindbrain. Intensity of Ca^{2+} signal is greater at the midline compared to the lateral regions. The three sites of whole-cell patch clamp are shown as colored circles. The propagation retracts laterally and medially at E13.5. Spontaneous activity disappears by E15.5. The X mark indicates hyperpolarization of the resting membrane potential in cells recorded from the region, demonstrating the progressive regional (or spatial) exclusion from spontaneous waves caused by hyperpolarization.

Possible mechanism of membrane hyperpolarization

There are several possible mechanisms for hyperpolarization to occur. First, the concentration gradient for ions may have changed. In the mouse spinal cord-hindbrain preparation, the disappearance of similarly synchronized electrical waves (which are different in origin and mechanism from those recorded in this study) are attributed to changes in the chloride concentration gradient (Momose-Sato *et al.*, 2012*a*; 2012*b*).

Our experiments argue against contribution of a shift in E_{Cl}. Clearly, hyperpolarization and change in resting conductance density was still observed even when the ion gradients were controlled within the cells recorded under whole-cell patch clamp.

Second, there may be upregulation of a new kind of ion channels that is open at rest. If this were true, we would predict resting conductance to increase. Indeed, this increase correlates both spatially and temporally with the retraction of spontaneous activity (Fig. 2.2, 2.5). A combination of both the hyperpolarization and the increased conductance would act to decrease membrane excitability, and this in turn would contribute to the retraction and cessation of the spontaneous activity.

If a new kind of ion channel is expressed, to what ion is it permeable? Because the membrane potential hyperpolarizes towards E_K (-97.4 mV) and away from E_{Cl} (-42.2 mV) (Fig. 2.2B, C), the channel is most likely to be permeable to K^+ ions. In support of this hypothesis, the membrane potential changed by the high $[K^+]_o$ ACSF followed E_K more closely at E15.5 (Fig. 2.3F). Since the linear IV relations follow Goldman-Hodgkin-Katz equation (Hille, 2001) at negative potentials (Fig. 2.2D), the channels are likely to be open at rest, typical of leak channels. A candidate leak channel, the two pore domain potassium (K_{2P}) family, fits this description. There are three K_{2P} channel types that appear to be present in the mouse hindbrain at E15.5 based on *in situ* hybridization: TREK-1, TREK-2 and TASK-3 (Aller & Wisden, 2008). A lack of specific pharmacological blockers for these channels makes it difficult to identify the functional presence of these channels.

At E15.5, gap junction blockers failed to prevent propagation of events evoked by high $[K^+]_o$ ACSF (Fig. 2.4B). This suggests that retraction may be caused by reduced

gap junctional coupling. While the present study does not fully explore this possibility, we think that changes in gap junctional coupling have a minor role in the retraction. As an example, if gap junctional coupling is reduced, the conductance should decrease. However, we observed just the opposite: there was an increase in the conductance (Fig. 2.2D, E). Even if gap junctional coupling was decreased, the corresponding decrease in the conductance may be masked by the increase in K^+ conductance, which is dominant.

Possible role for spontaneous activity retraction

Spontaneous activity plays an important role in the formation of neuronal circuits, and it has been reported to affect proliferation, migration, differentiation, axonal guidance, synaptogenesis and ion channel expression (Moody & Bosma, 2005; Spitzer, 2006; Hanson *et al.*, 2008). The retraction and cessation of activity may have several crucial consequences on circuit development. First, it is possible that spontaneous activity regulates cellular proliferation or migration. Between E10.5 and E15.5, the hindbrain changes thickness of the tissue from the ventricular zone to the pial surface, indicative of continued proliferation during periods at which the spontaneous activity is present (data not shown). Perhaps this process requires calcium influx, as has been shown to occur in developing neocortex (Weissman *et al.*, 2004), and retraction and disappearance of spontaneous activity may signal cessation of cell proliferation across the hindbrain.

It is also possible that the circuit is changing from a gap junction-based system to an adult form of neuronal communication: synaptic transmission. This transition may

take time even after spontaneous activity disappears because the circuitry at E15.5 still seems to support propagation of events, as evidenced by the induction of events using high $[K^+]_o$ ACSF (Fig. 2.4). However, this propagation already appears to be independent of gap junctional coupling (Fig. 2.4B), which is required for synchronization at earlier stages (Hunt *et al.*, 2006*a*). Data from the Allen Brain Atlas (http://www.brain-map.org) demonstrates that mRNAs encoding synaptic proteins such as syntaxin-1, synapsin I, and the presynaptic $Ca_v2.1$ channel are detected in high levels starting on or after E15.5. In addition, a large number of glutamate receptors become upregulated at E15.5. Acute bath application of 2 μM AMPA can evoke propagating events along the midline of quiescent hindbrain at E14.5-E15.5 (n=5, data not shown), but the activated glutamatergic receptors may include extrasynaptic sites. More work needs to be done to determine whether the mouse hindbrain support synaptic transmission at or after E15.5, coinciding with the cessation of spontaneous activity.

We have demonstrated that the spontaneous activity recorded in the E11.5 hindbrain undergoes a characteristic spatial and temporal retraction mediated by progressive hyperpolarization of the resting membrane potential and increase in resting conductance. The last region to undergo these changes is the InZ, which retains the ability to support events until relatively late in development. The fact that events can be induced in midline cells by membrane depolarization, and that resting membrane potential is more closely set by E_K than E_{Cl}, suggests that changes in expression of resting K^+ conductance may be crucial in the spatiotemporal regulation of spontaneous activity.

Proper development of neuronal circuits requires spontaneous activity, but as the circuits mature, the system needs to desynchronize activity to switch from widespread network propagation to local information processing. Reducing membrane excitability by hyperpolarization of the resting membrane potential and increasing resting conductance are effective mechanisms to desynchronize activity in a spatiotemporal manner, while allowing information processing to occur at the synaptic and cellular level. Since spontaneous activity raises $[Ca^{2+}]_i$, the retraction sequence itself may be regulated by gene expression. Calcium influx that results from spontaneous activity may upregulate expression of resting ion channels, suppressing subsequent Ca^{2+} influx by membrane hyperpolarization and increased resting conductance, effectively turning off spontaneous activity in a feedback loop. At the same time, the influx of Ca^{2+} may also upregulate synaptic proteins and prepare individual neurons to support synaptic transmission as the primary form of cellular communication.

Acknowledgments

Special thanks to Amanda Tose (co-author of this work), Bess Navarrete, Mark Shi, Lucy Liu, Bethanny Danskin, Veronica Rodriguez, Ashley Lin and Joseph Bosma-Moody for technical assistance, and to Bill Moody for critical reading of the manuscript. This work is supported by NSF IOS 0952395.

Chapter 3: Looping circuit: a novel mechanism for prolonged spontaneous intracellular calcium increases in developing embryonic mouse brainstem

Introduction

Calcium is a unique ion that acts not only as a charge carrier mediating membrane excitability but also as a second messenger modulating cellular processes such as gene expression. In many regions of the developing mammalian nervous system including the brainstem (Bosma, 2010), calcium is introduced into the cytoplasm by spontaneous activity, which plays an important role in developmental processes such as proliferation, differentiation, migration, axonal pathfinding, synaptogenesis and neurotransmitter respecification (Moody and Bosma, 2005; Spitzer, 2012).

Spontaneous activity occurs during embryonic days (E) 10.5-E13.5 in the mouse brainstem (Hunt *et al.*, 2006*b*; Rockhill *et al.*, 2009). Most events originate in an area called the initiation zone (InZ) (Moruzzi *et al.*, 2009), which is located at the midline of the hindbrain about 50 μm rostral to the trigeminal nerve exit point in former rhombomere (r) 2. After initiation, events propagate rostrocaudally along the midline of the hindbrain (Hunt *et al.*, 2006*b*). At E12.5, some events propagate rostrally across the midbrain-hindbrain border (isthmus) and into the midbrain tegmentum. This propagation putatively occurs via tracks made by axons of serotonergic neurons that extend rostrally through that region (Rockhill *et al.*, 2009). From E13.5-E14.5, the extent of propagation shrinks and events finally disappear due to a progressive increase in the resting potassium conductance and hyperpolarization of resting membrane potential (Watari *et al.*, 2012).

Spontaneous activity is driven by membrane depolarization, which activates Ni^{2+} and mibefradil-sensitive Ca_V3 channels mediating T-type Ca^{2+} current (Moruzzi *et al.*, 2009). This membrane depolarization resembles a conventional action potential in that it often overshoots 0 mV when beginning from a relatively hyperpolarized resting membrane potential. Unlike a conventional action potential, however, the depolarization that underlies spontaneous activity consists of a brief spike followed by a long plateau, and it lasts for up to 1 s before the membrane repolarizes to rest (Moruzzi *et al.*, 2009). The resting membrane potential can range widely, from -35 mV to -80 mV, depending on the stage and location in the hindbrain; cells positioned closer to the InZ show more depolarized potentials during the window of spontaneous electrical activity (E11.5-E13.5) (Watari *et al.*, 2012). This suggests that a relatively more depolarized resting membrane potential may prime InZ cells to fire spontaneously. Each depolarization leads to, and is outlasted by, an increase in $[Ca^{2+}]_i$, causing each calcium event to last approximately 6 s (Watari *et al.*, 2012).

Here, we report a novel mechanism that underlies a previously uncharacterized phenomenon called Bash Bursts (Bash-B), in which $[Ca^{2+}]_i$ rises above baseline for, in some cases, tens of minutes, an unusually long time. We show that a looping circuit is an effective mechanism by which participating cells can experience calcium influx at frequent and regular intervals. Bash-B emerges at E12.5, and it disappears within 24 hours due to alteration of the looping circuit, making Bash-B stage-specific. These bouts of sustained increase in $[Ca^{2+}]_i$ may modulate gene expression that is necessary for the development of the rostral brainstem, including the raphe serotonergic and tegmental dopaminergic neurons that develop along the paths of spontaneous activity.

Methods

Animals and Dissections

All animal care procedures were approved by University of Washington Animal Care Committee (IACUC). Timed-pregnant Swiss/Webster mice were sacrificed by CO_2 followed by cervical dislocation. Embryos from E10.5-E15.5 were maintained in ACSF, containing (mM): 119 NaCl, 2.5 KCl, 1.3 $MgCl_2$, 2.5 $CaCl_2$, 1 NaH_2PO_4, 26 $NaHCO_3$, 30 glucose, oxygenated with carbogen (5% CO_2, 95% O_2). When the brainstem (midbrain, hindbrain and cerebellar flap) was dissected out, the hindbrain naturally laid flat in an open-book configuration; the midbrain was cut along its dorsal midline so that it laid flat along with the hindbrain. Some calcium imaging recordings were done on brainstem preparations with spinal cord attached. Some patch clamp recordings that didn't require midbrain were performed on isolated hindbrains. The mesenchyme was removed in all preparations with one exception; a small patch of mesenchyme was left attached on some E11.5 brainstem preparations around the midbrain tegmentum area to avoid pulling on cranial nerve III and damaging the area. The dissected tissue was bath perfused in oxygenated ACSF at the rate of 1 mL ± 0.3/min. Osmolarity of the oxygenated solution was 316 ± 1 mosmol/L. All experiments were done at approximately 23 ˚C.

Calcium imaging

The brainstem was dissected out and incubated in oxygenated ACSF with 1.9 μM Quest Fluo-8-AM (AAT Bioquest, Inc., Sunnyvale, CA) and 0.075% Pluronic F-127

(Sigma-Aldrich, St. Louis, MO) for 15 min at 23 ˚C. Changes in fluorescence were measured in up to 83 regions of interest (ROIs) using a 10X objective for r2 InZ experiments and a 4X objective for midbrain-hindbrain experiments. ΔF/F values were recorded using Metafluor (Molecular Devices, LLC., Sunnyvale, CA) with shutter speeds of 1 Hz or 2.43 Hz. Flupirtine was dissolved in ethanol at a stock concentration of 10 mM, and stored at -20 ˚C. Data were visualized and analyzed using ImageJ (National Institutes of Health, Bethesda, MD), Excel (Microsoft Corp., Redmond, WA), and Igor Pro (Wavemetrics, Inc., Lake Oswego, OR) with custom functions developed by Hirofumi Watari. For line intensity scan analysis, individual pixels from image sequences containing 2-5 propagating events were compiled into a single image based on the value of the highest intensity recorded at each pixel. The resulting image was smoothed by the Gausian bicubic method. The line scan was performed across the midline axis every 200 μm from isthmus to r2 on the hindbrain and across midbrain tegmentum 100 μm rostral to the isthmus; each line scan was repeated over the rostrocaudal area covering 20 x 400 μm^2 and the averaged result was then plotted. Statistics for the correlation analysis was done using Pearson's r.

Electrophysiology

Internal solution contained the following (mM): 100 K-gluconate, 15 KCl, 1 EGTA, 5 $MgCl_2$, 40 HEPES, 3 Na-ATP, 0.3 Na-GTP. pH was titrated to 7.25 by addition of NaOH. Osmolarity was adjusted to 328 ± 2 mosmol / L by addition of sucrose. Some patch clamp experiments were done on isolated hindbrain preparations with the midbrains removed, but the results did not differ from recordings done on midbrain-

hindbrain preparations, thus all data were pooled. For voltage-step experiments, P/-4 leak subtraction was applied online to expose a component of current that is voltage-dependent. Data were acquired using pCLAMP (Molecular Devices, LLC., Sunnyvale, CA) under the same conditions as described previously (Watari *et al.*, 2012). Data were analyzed using Igor Pro with custom functions provided by Hirofumi Watari and NeuroMatic (Jason Rothman). All statistics, unless indicated otherwise, were one-way analysis of variance (ANOVA). If the result of group comparison was significant, multiple comparison Tukey (HSD) test was performed *post-hoc*. *p<0.05, **p<0.01, ***p<0.001.

Results

Sustained intracellular calcium in midline cells of rostral brainstem at E12.5

Spontaneous activity originates at the initiation zone (InZ), which is predominantly located along the midline of former rhombomere (r) 2 (Fig. 3.1A, gray box) (Hunt *et al.*, 2006*a*; Moruzzi *et al.*, 2009). This spontaneous activity is a distinct phenomenon from a variant of depolarization waves that originates in the spinal cord (Momose-Sato *et al.*, 2012) because the location of the InZ is unaffected by removal of the spinal cord. At E12.5, events originating from the InZ can be followed by a bout of high frequency calcium events arriving from the rostral midline of the hindbrain. An example of this is shown in Figure 3.1B, where a train of four calcium waves propagate caudally after an InZ-initiated event (*; event not shown), with wavefronts spaced approximately 300 μm apart from each other (calcium events labeled a, b, c, d in panels 1.2 s-14.8 s of Fig. 3.1B). This train of calcium events summate (Fig. 3.1C, middle).

This type of summated bursting of Ca transients is most prevalent at E12:5: it has been observed at E11.5 (n=3 of 18 experiments), although most events occur from a defined baseline (Fig. 3.1C, left) at a frequency of 3.2 ± 0.2 events per minute (Hunt *et al.*, 2006*b*), while at E13.5, events occur less frequently, 1.9 ± 0.3 events per minute (Hunt *et al.*, 2006*b*), and do not summate (n=8) under normal conditions (Fig. 3.1C, right). Here, we characterize the high frequency $[Ca^{2+}]_i$ events seen at E12.5.

Within these trains, each event peak is followed by another peak before the $[Ca^{2+}]_i$ returns to baseline, and as a result the midline cells experience above-baseline $[Ca^{2+}]_i$ for a mean of 79.47 ± 8.15 s (n=206, 62 preparations); the longest episode lasted 12 min 19 s (Fig. 3.1D). These instances of high frequency $[Ca^{2+}]_i$ events are called Bash Bursts (Bash-B). Bash-B occurs in 78.9% of E12.5 litters (30 out of 38 litters, recording from 3 or more brainstems per litter). Of those litters, 58.1% brainstem preparations (n=61 out of 105 total) showed an average of 3.44 ± 0.29 separate instances of Bash-B while the remaining preparations did not show Bash-B during the 30 min recording period. Each tissue that can show Bash-B spends 15% (4 min 34 s of the 30 min recording period) undergoing Bash-B, leading to sustained $[Ca^{2+}]_i$.

Events that resulted in Bash-B were arriving from a more rostral region than former r2 (Fig. 3.1B). To investigate where these events originate and how their frequency is set, we performed calcium imaging using a low magnification objective (4X) to view the InZ as well as rostral regions up to and including the midbrain tegmentum (Fig. 3.2).

A typical episode of Bash-B begins with an event that initiates at the InZ (* at 0 s in Fig. 3.2). The InZ is located exclusively in the hindbrain (n=25), as reported

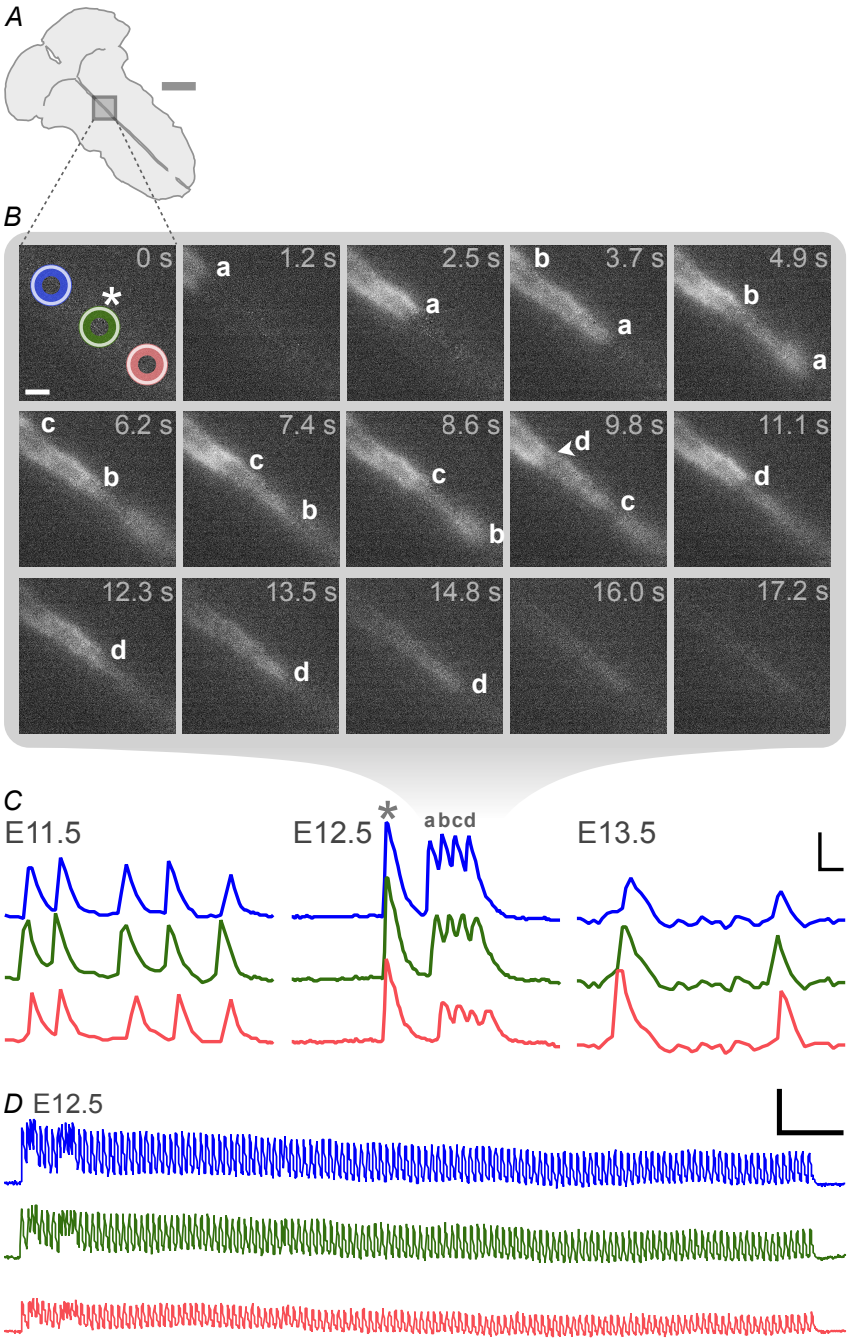

Figure 3.1. A sustained increase in $[Ca^{2+}]_i$ in the midline of the hindbrain at E12.5
A, Position of $[Ca^{2+}]_i$ imaging on r2 of the hindbrain midline. Scale bar: 1 mm. B, Image sequence of high frequency spontaneous activity recorded at E12.5. Position of event initiation (not shown in this sequence) is indicated as * at 0 s. Change in fluorescence is measured in three regions of interest (ROIs), placed along the midline as shown at 0 s. The colors of the ROIs correspond to the colors of ΔF/F *vs.* time traces shown in panels C and D below. Recurrent calcium waves, indicated as a-d, propagate caudally along the midline of hindbrain (1.2-17.2 s); each wavefront appears from a more rostral part of the hindbrain (off screen in upper left corner of the image). Scale bar: 100 μm. C, Representative patterns of $[Ca^{2+}]_i$ events plotted as ΔF/F vs. time from E11.5-E13.5, demonstrating different wave patterns at each of the 3 stages. At E11.5 (left), most $[Ca^{2+}]_i$ waves are recorded as single, discrete events. At E12.5 (middle), an event at the initiation zone (InZ; labeled *) is followed by multiple calcium waves that occur in rapid succession (labeled a-d); the resultant $[Ca^{2+}]_i$ events summate such that each peak in $[Ca^{2+}]_i$ occurs before $[Ca^{2+}]_i$ from the previous event returns to baseline. This episode of sustained $[Ca^{2+}]_i$ is referred to as Bash-B. At E13.5 (right), events become less frequent and, as also observed at E11.5, do not summate. Scale bar: 3 ΔF/F and 5 s. D, One of the longest recorded durations of Bash-B is over 12 min, encompassing 129 calcium wave propagations. Scale bar: 3 ΔF/F and 1 min.

previously (Rockhill *et al.*, 2009), although some initiations occurred more rostrally along the midline of the hindbrain in between isthmus and r2. An example of Bash-B is characterized by the following sequence. An event originates at the InZ and propagates rostrally along the midline (Fig. 3.2, 1.2-4.9 s) until it reaches the midbrain-hindbrain boundary, or isthmus (Fig. 3.2, dashed box; also see Fig. 3.3 at 4.9 s), and crosses it. After the event crosses the isthmus (Fig. 3.3, 5.7 s), it propagates first on the right side of the midbrain (Fig. 3.3, 6.2-6.6 s). The event then crosses the midline to reach the left side of the midbrain (Fig. 3.3, 7.0-7.8 s) and exits the midbrain by re-crossing the isthmus and propagating back into the hindbrain (Fig. 3.3, 8.2 s). The event propagates caudally on the left side of the hindbrain midline (Fig. 3.3, 8.6-9.0 s), crosses over to the right side of the midline (Fig. 3.3, 9.4 s), and then bifurcates so that the event propagates both rostrally and caudally (Figs. 3.2 and 3.3, 9.8 s). The caudally-directed component propagates along the midline tracks, passes through the InZ, and dissipates (Fig. 3.2, 11.1-16.0 s; bottom half of the panels). The other component propagates rostrally, reenters the midbrain, and the looping process repeats itself (9.8 s and later in Figs. 3.2 and 3.3). Several loops from this episode are shown at higher temporal resolution in Figure 3.3, demonstrating the repetitive circular pattern of propagation at or near the isthmus. In this case, the event took approximately 5 s to loop around once. The $[Ca^{2+}]_i$ peaks every 5 s in the midline cells, shorter than the amount of time it takes for $[Ca^{2+}]_i$ to return to baseline, resulting in Bash-B. This 5-s propagation pattern is referred to as the midbrain-hindbrain loop (Fig. 3.4A) because it involves a circuit that encompasses both the midbrain and the hindbrain with the isthmus border acting as a “pivot” at the midline, around which the event propagates.

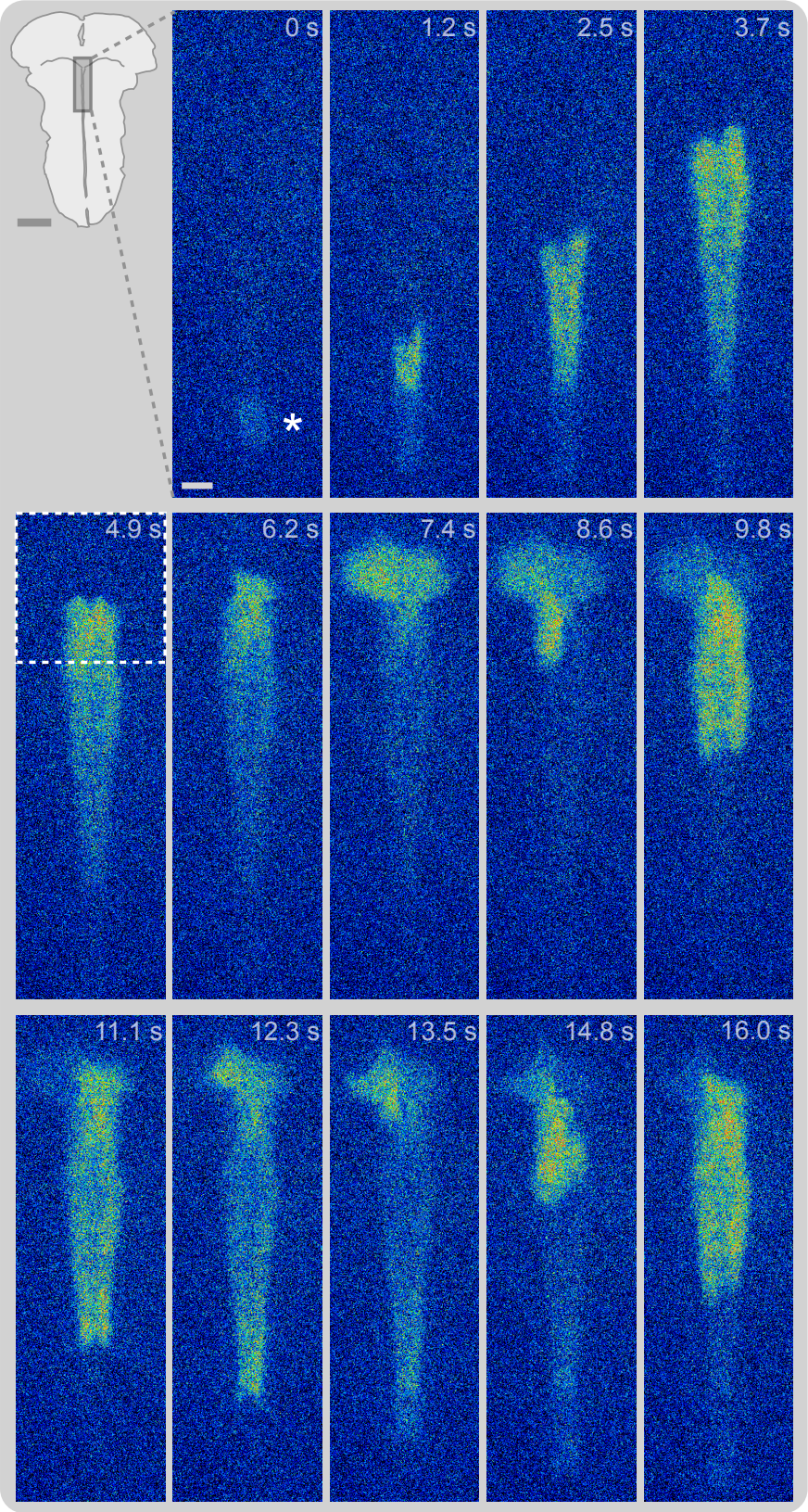

Figure 3.2. Bash-B is a result of a looping calcium event at E12.5
Calcium imaging along the midline of the rostral brainstem using a low magnification objective (4X) so that the InZ (* at 0 s) at r2 hindbrain and the midbrain tegmentum are included; camera position is indicated at the upper left corner (Scale bar: 1 mm). Panels of image sequences are shown starting at 0 s, when $[Ca^{2+}]_i$ event initiates at the InZ (*). The event then propagates rostrocaudally (1.2 s), with the caudal portion disappearing from the bottom of the image (2.5 s). The event propagates rostrally (1.2-3.7 s) until its wavefront reaches the midbrain-hindbrain border, or isthmus (4.9 s). A sequence of higher temporal resolution image in the squared area (dotted line at 4.9 s) is captured in Figure 3.3 to show the details of calcium wave propagation. The event enters the midbrain tegmentum (6.2 s), propagates contralaterally (7.4 s), crosses the isthmus caudally and propagates back into the hindbrain (8.6 s), and then splits so that one portion of the event propagates caudally (9.8-16.0 s), while the other portion propagates rostrally. The rostral portion then reenters the midbrain (9.8 s), again propagates contralaterally across the midbrain (11.1-13.5 s), crosses the isthmus (14.8 s), and the whole cycle repeats itself (16.0 s). The images are pseudo-colored to show relative intensity of $[Ca^{2+}]_i$ for clarity (low fluorescence: blue, high fluorescence: red). Scale bar: 100 μm.

Whereas some loops involve tracks in both the midbrain and the hindbrain (Fig.

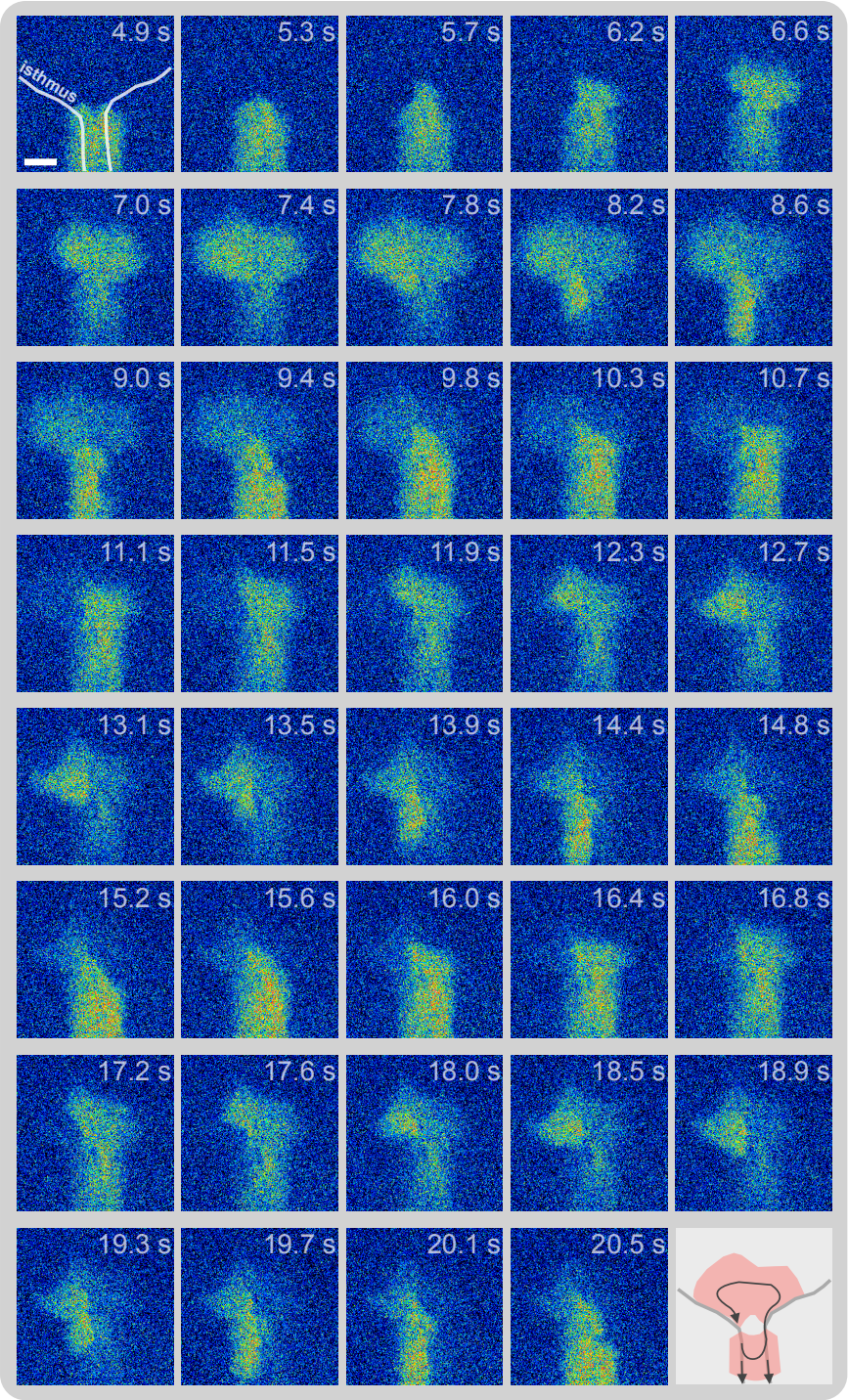

Figure 3.3. Midbrain-hindbrain loops underlie Bash-B and have a characteristic 5-s lap time
A looping circuit involving paths in the midbrain tegmentum and rostral hindbrain, imaged at high temporal resolution. The outline of the midbrain-hindbrain border (isthmus) and the two midline tracks in the hindbrain (vertical lines) are shown in the image at upper left corner. The image sequence is taken directly from the squared area in Figure 3.2 at 4.9 s. The calcium event propagates rostrally and crosses the isthmus at 5.3 s. The wavefront enters the midbrain tegmentum (5.7 s) and propagates on the right side of the midbrain tegmentum (6.2 s). It then propagates contralaterally to the left side of the midbrain (6.6-7.8 s), crosses the isthmus (8.2 s), and propagates caudally on the left midline track in the hindbrain (8.2-8.6 s). The event propagates contralaterally to the right midline track in the hindbrain (9.0-9.4 s) and bifurcates so that events propagate rostrocaudally along that right track. The rostral portion of the event crosses the isthmus, and the cycle repeats itself twice more counter-clockwise (9.8-15.2 s and 15.6-20.5 s). Note that each lap takes approximately 5 s. Lower right: an illustration of the looping track (salmon colored area) and the direction of event propagation (arrows). Scale bar: 100 μm.

3.4A), other loops occur exclusively in the hindbrain (hindbrain-only loops) (Fig. 3.4B). Location is not the sole difference between these two types of loops; another critical difference is the lap time. While the mean lap time is 4.98 ± 0.29 s (n=7) for the midbrain-hindbrain loops, the lap time is significantly faster for the hindbrain-only loop

(2.95 ± 0.17 s, n=7; $p<0.001$). The consequence of a faster lap time is that it reduces the interval during which the cell can extrude cytoplasmic calcium before the next event arrives, therefore the participating cells experience a higher average $[Ca^{2+}]_i$, closer to its peak $\Delta F/F$ value; this is in contrast to Bash-B with larger deflections in $[Ca^{2+}]_i$ caused by the midbrain-hindbrain loops. These distinct lap times are useful markers to predict the type of looping circuit during patch clamp experiments where spatial information of the event propagation is absent.

A few episodes of Bash-B does not involve a looping circuit, but instead results from rapid repetitive firing at the InZ (Fig. 3.4C, left half). Bash-B can also result from a combination of the above mechanisms. Examples exist where it can switch from rapid firing of the InZ to midbrain-hindbrain loops (Fig. 3.4C), or from midbrain-hindbrain loops to hindbrain-only loops (Fig. 3.4D), yielding $[Ca^{2+}]_i$ peaks at different intervals. Other combinations of the various submodalities of Bash-B are also possible. The directionality of the loop can either be clockwise or counter-clockwise, and a given preparation is capable of looping in either direction (Fig. 3.4D). However, the directionality is not entirely random for certain types of loops, which will be described in detail below.

Directionality is predictable for hindbrain-only loops

The brainstem inherently allows the event to loop either clockwise or counter-clockwise, but after the first lap the event tends to continue to loop in the same direction. The directionality is predictable for the shorter (3-s) hindbrain-only loops, but not for the longer (5-s) midbrain-hindbrain loops. For the 3-s loops, the directionality is

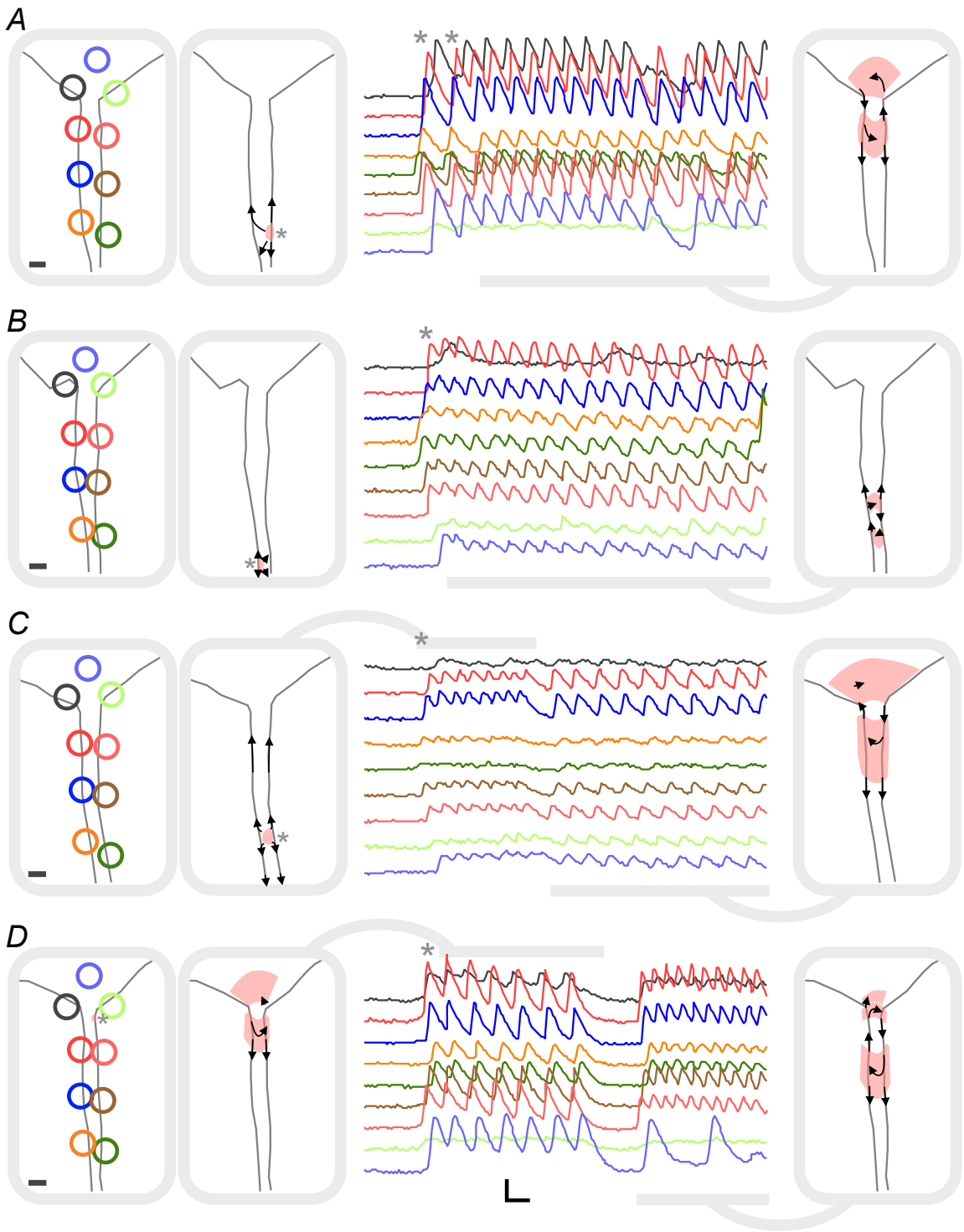

Figure 3.4. Variations of loops that underlie Bash-B
Four examples of Bash-B at E12.5. Every instance of Bash-B follows an initiating trigger (*) in the hindbrain, and, with some exceptions, is comprised of one or more loop patterns. A, Midbrain-hindbrain loops. B, Hindbrain-only loops. C, A non-looping, rapid firing of InZ followed by midbrain-hindbrain loops. D, Counter-clockwise midbrain-hindbrain loops followed by clockwise hindbrain-only loops. During the latter, the event enters the midbrain tegmentum only sporadically (light blue trace). A-D, ROIs in the left panels correspond to the color-matched ΔF/F traces. Scale bar: 100 μm. All traces: Representative ΔF/F traces showing Bash-B. Scale bar: 2 ΔF/F and 5 s. Panels to the sides of the traces illustrate the patterns of event propagation. The length of the arrows in the diagrams shows relative speed of propagation, where a short length indicates slower propagation. Illustrations depicting the looping tracks, locations of the InZ, and directionality were created after video analysis, as in Figure 3.3.

well correlated with the side of the midline at which the event initiates (r=0.76). When events initiate on the left side of the midline, they consistently loop clockwise (n=4 of 4; Fig. 3.4B) whereas events that initiated on the right side turn counter-clockwise (n=4 of 5). Thus, for hindbrain-only loops, 88.9% (n=8 of 9) of the directionality is set by the location on the midline at which the event initiates. In contrast, the directionality is less predictable for the 5-s midbrain-hindbrain loops (r=-0.31) with a lower probability of 36.4% (n=4 of 11). An unknown process in the midbrain, perhaps related to refractoriness, seems to allow the event to turn either direction and to even reverse direction.

Membrane excitability peaks in InZ cells at E12.5

The midline cells, including the cells at the InZ, have lower resting conductance and more depolarized resting membrane potential (V_{rest}) compared to lateral cells. This makes them more excitable and supportive of spontaneous firing (Watari *et al.*, 2012). Additionally, the midline cells display a relatively large voltage-gated inward current, which supports depolarization (Moruzzi *et al.*, 2009). However, Bash-B is a phenomenon that is most prevalent at E12.5, and a possible change in the excitability of the cells at the InZ may underlie its ability to sustain activity at the frequencies of the loops. We therefore performed voltage clamp on InZ cells from E11.5-E13.5. In order to plot the activation curve for the inward current, the voltage was stepped from -80 mV to +80 mV in 5 mV increments; peak inward current (occurring within the first 34 ms) was measured and plotted against voltage (Figs. 3.5A-C, open circles).

At early stages, the predominant inward current is T-type calcium (Moruzzi *et al.*, 2009), but starting at E12.5, the inward current appears to be a combination of Ni^{2+}-sensitive calcium current and TTX-sensitive sodium current (n=3, data not shown). The voltage-gated ion channel that mediates the inward current inactivates rapidly with a mean time constant of 4.68 ± 0.97 ms (n=15; the voltage was stepped from -80 mV to -10 mV). We measured the residual inward current after a prepulse and plotted the steady state inactivation at each stage. The resulting inactivation curve (closed squares) is superimposed on the activation curve (Figs. 3.5A-C). This exposes the "window current" (Figs. 3.5D-F), a persistent inward current that is known to occur for certain types of calcium current including the T-type (Capiod, 2011). The window current occurs in the range of voltages from -6.27 ± 2.90 mV to -46.23 ± 2.17 mV at E12.5 (n=16), within which there is a net inward current (peaking at -30.90 ± 0.96 mV) (Fig. 3.5G). At E12.5, the peak inward current increases significantly (E11.5: -178.36 ± 20.85 pA, n=18 *vs.* E12.5: -289.34 ± 39.85 pA, n=16; $p<0.05$), as does the peak window current (E11.5: -40.87 ± 4.68 pA, n=18 *vs.* E12.5: -97.71 ± 22.13 pA, n=16; $p<0.05$) (Fig. 3.5H). This indicates that the midline cells at E12.5 can support robust spontaneous membrane depolarization. In addition, the peak inward current density reaches its highest value at E12.5 (Fig. 3.5I), indicating that a relatively high density of voltage-gated ion channel types that mediate inward current is expressed at this stage. As shown by the arrows (Figs. 3.5D-F), at every stage, the mean resting membrane potential (Watari *et al.*, 2012) lies within the voltage range of window current, suggesting that calcium may leak into the cytoplasm even at rest, contributing to spontaneous activity. Therefore, window current may play a role in initiating spontaneous activity and

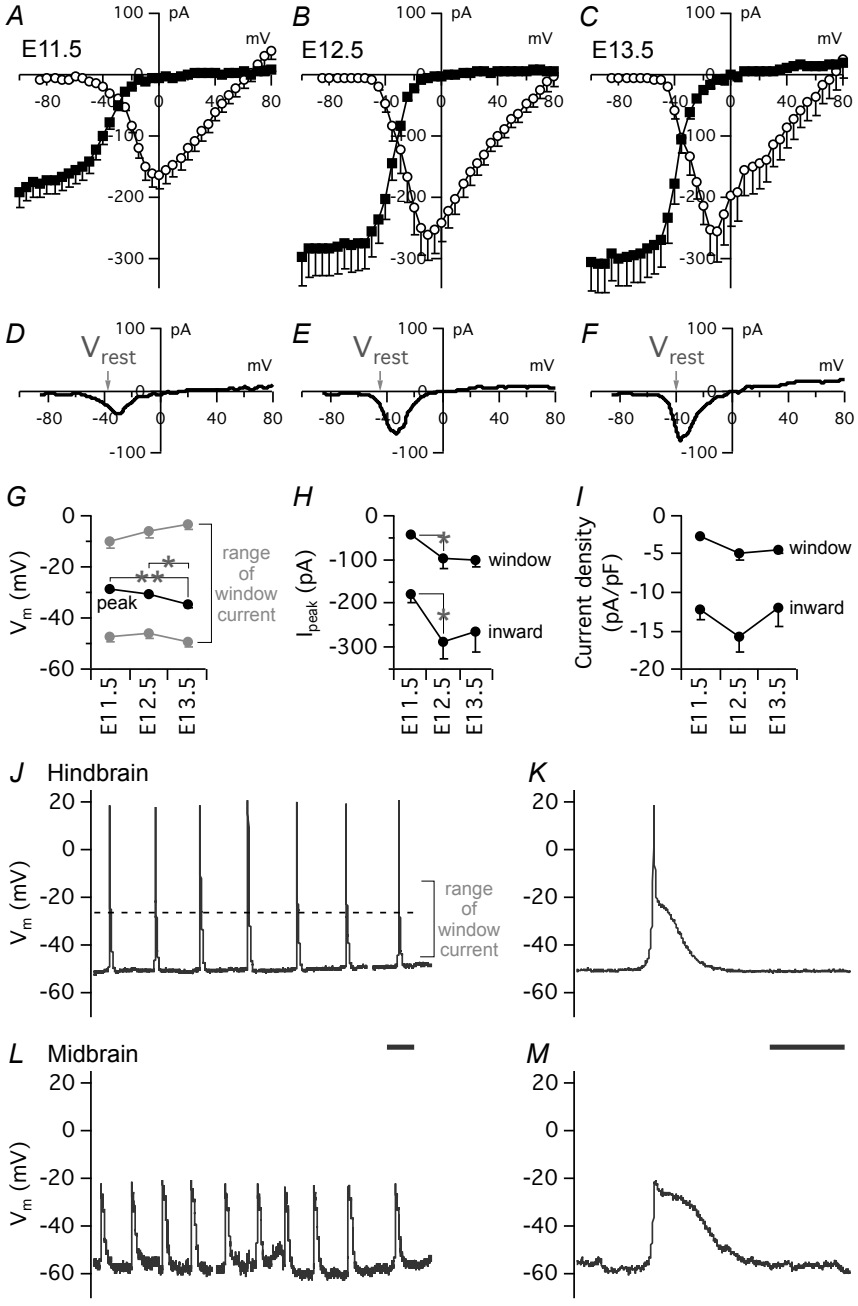

Figure 3.5. Window current peaks at E12.5 and makes InZ cells more excitable
Superimposed activation (open circle) and inactivation (closed square) current-voltage (IV) relations for voltage-gated inward current shown for E11.5 (A), E12.5 (B), and E13.5 (C). D-F, IV relations for the averaged window current, extracted from the superimposed activation and inactivation curves above. Mean V_{rest}, adapted from Watari *et al.*, 2012, is indicated by arrows on the voltage axis. G, upper and lower voltage ranges of window current (gray) and voltage at which the window current peaks (black) at each stage. H, peak window current and peak inward current at each stage. I, current densities (pA/pF) for peak window and peak inward current at each stage. G-I, E11.5: n=18; E12.5: n=16; E13.5: n=7. The error bars are SEM. J, a representative current clamp trace recorded from a midline cell in r1 hindbrain during midbrain-hindbrain loops. K, waveform of a depolarizing event sampled from panel J (third event). L, a representative current clamp trace recorded from a midline cell in midbrain tegmentum during midbrain-hindbrain loops. M, waveform of a depolarizing event sampled from L (third event). Scale bar: 5 s (J, L) and 1 s (K, M).

setting V_{rest} itself by counterbalancing leak outward current. The increase in peak inward current and window current, coupled with relatively lower resting conductance (Watari *et al.*, 2012), makes the InZ cells at E12.5 one of the most excitable cells in this system across stages, and thereby make them uniquely able to support event initiation necessary for Bash-B.

The existence of window current suggests that the InZ cells could undergo sustained influx of calcium, resulting in Bash-B, by persistent membrane depolarization near the voltage of peak window current (-30.90 ± 0.96 mV at E12.5, n=16) (Fig. 3.5G). We investigated this possibility by performing current clamp of an r1 hindbrain cell, which is typically included in the pathway of Bash-B propagation. The recording shows an example of membrane potential during a midbrain-hindbrain loop (Fig. 3.5J). Each depolarizing event shows a characteristic waveform with a fast-rising peak that overshoots 0 mV followed by a slower plateau (Fig. 3.5K) (Moruzzi *et al.*, 2009). Instead of holding the voltage around the peak of window current (dotted line in Fig. 3.5J; -26.37 mV for this cell), each depolarizing event repolarizes fully back to V_{rest} (-49.64 ± 0.40 mV for this cell) before the next depolarization. The trace is unlike the Bash-B seen in calcium imaging where consecutive peaks occur before they can return to baseline. Therefore, the fact that $[Ca^{2+}]_i$ remains above baseline during Bash-B episode is probably not due to persistent depolarization of membrane potential, but to an interval between membrane potential depolarizations shorter than the extrusion time of calcium.

Midbrain cells are less excitable than hindbrain cells at E12.5

Similar to the hindbrain cells, current clamp of a midline cell in the midbrain tegmentum (150 μm rostral to the isthmus, within the looping circuit) shows each depolarizing event returning to the resting membrane potential during a midbrain-hindbrain loop (Fig. 3.5L). However, midbrain cells exhibit smaller peak amplitudes and longer plateaus than hindbrain midline cells (Fig. 3.5M compared to 3.5K). This

suggests that the midbrain cells have different membrane properties than the hindbrain cells. To test this, we performed voltage clamp at three locations along the midline of the rostral brainstem, as shown in Figure 3.6A: midbrain tegmentum 150 μm rostral to the isthmus (MB); hindbrain r1 (r1); hindbrain r2 (r2). Because the midbrain cells have a smaller membrane capacitance compared to the hindbrain cells (Fig. 3.6C), indicating smaller cell diameter, we calculated current densities per unit capacitance. The peak inward current and the peak window current were both smaller in midbrain cells than in hindbrain cells (Figs. 3.6B, D, F). The inward current density for midbrain cells (-5.96 ± 0.74 pA/pF, n=13; $p<0.001$) is one third of that for hindbrain cells (r1: -16.36 ± 1.24 pA/pF, n=10; r2: -15.68 ± 2.00 pA/pF, n=16) (Fig. 3.6E), and the window current density is about half (Fig. 3.6G; MB: -2.81 ± 0.21 pA/pF, n=13; r1: -4.61 ± 0.81 pA/pF, n=10; r2: -4.82 ± 0.89 pA/pF, n=16; p=0.11), suggesting that there are fewer voltage-gated ion channels that support depolarization in the midbrain. The outward current is similar in midbrain and hindbrain cells (Fig. 3.6H; MB: 353.65 ± 39.62 pA, n=13; r1: 469.39 ± 44.48 pA, n=10; r2: 334.51 ± 35.91 pA, n=16; V_{hold}=+80 mV; p=0.063), but when normalized to membrane capacitance, the resulting outward current density is significantly higher in the midbrain cells (Fig. 3.6I; MB: 34.67 ± 2.74 pA/pF, n=13; r1: 22.66 ± 1.64 pA/pF, n=10; r2: 18.44 ± 1.50 pA/pF, n=16; MB *vs.* r1, $p<0.01$; MB *vs.* r2, $p<0.001$). Taken together, the midbrain cells have a higher density of voltage-gated ion channels that hyperpolarize rather than depolarize, which is consistent with the observation that spontaneous activity initiates in the hindbrain but not in the midbrain (Rockhill *et al.*, 2009). Also, this lower excitability may explain the slower propagation of

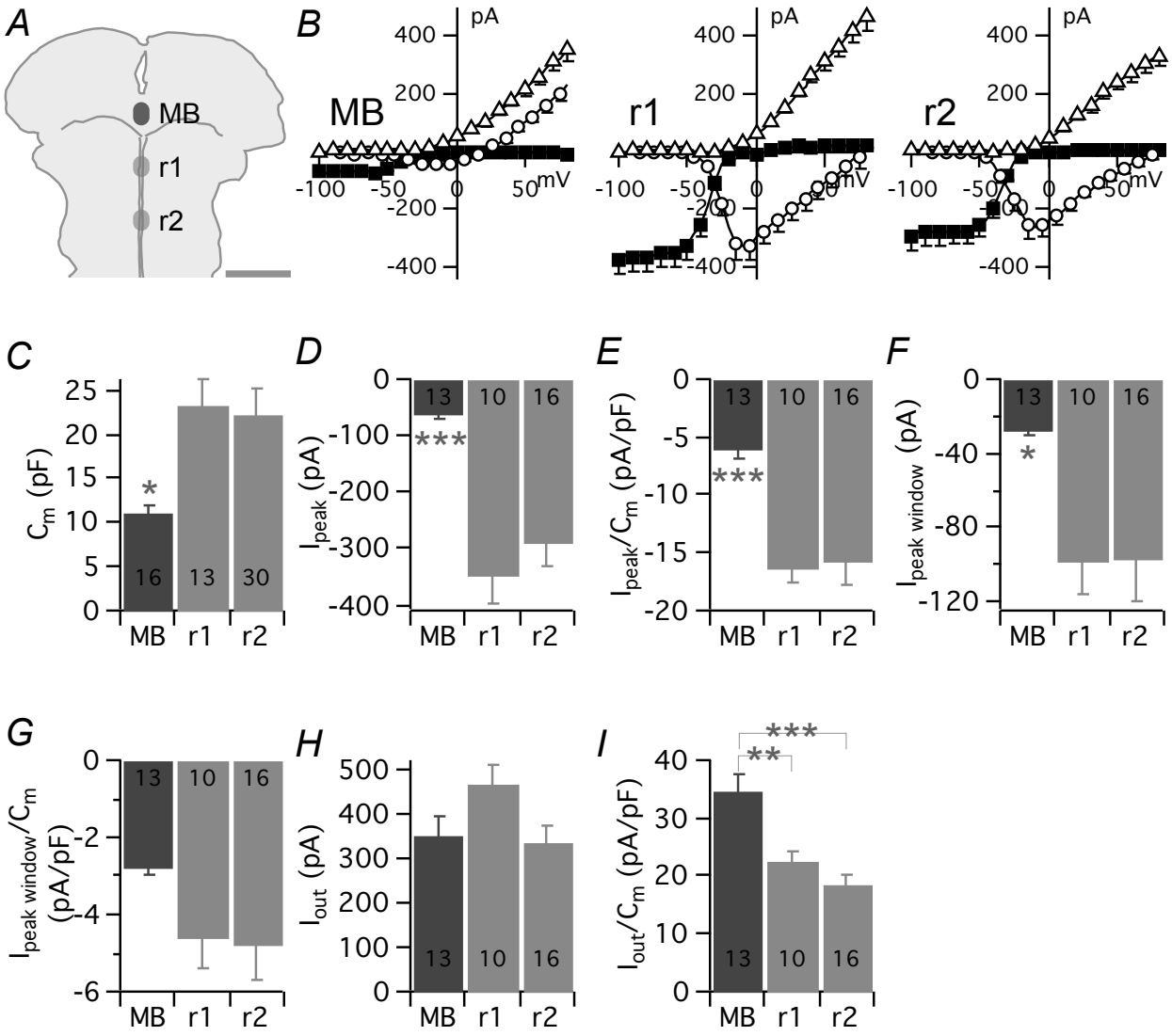

Figure 3.6. Midbrain cells are less excitable than hindbrain cells at E12.5, expressing less inward and more outward current densities

A, Sites of patch clamp recordings: midbrain tegmentum 150 μm rostral from isthmus and along midline axis (MB); r1 hindbrain 250-350 μm caudal from isthmus and 50 μm lateral to the midline axis, closer to one of the two parallel tracks (r1); r2 hindbrain 50 μm rostral to cranial nerve V and along midline axis, closer to one of the two parallel tracks (r2). Scale bar: 1 mm. B, Superimposed activation curve for voltage-dependent inward current (open circle), inactivation curve for voltage-dependent inward current (solid square), and activation curve for voltage-dependent outward current (open triangle). C, Membrane capacitance. D, Peak inward current. E, Peak inward current density. F, Peak window current. G, Peak window current density. H, Peak outward current. I, Peak outward current density. C-I, n≥10 at each stage. The error bars are SEM.

events in the midbrain tegmentum during Bash-B, which may contribute to the slower lap time in the loops that involve the midbrain.

Bash-B ceases by E13.5, can it be rescued?

Membrane properties of midline cells are similar between E12.5 and E13.5 (Figs. 3.5B-C, E-F, H-I). This suggests that Bash-B could be supported at E13.5. However, Bash-B disappears by E13.5. One major difference between E12.5 and E13.5 is that outward current is larger at E13.5 (568.65 ± 76.06 pA at E13.5, n=7 *vs.* 334.51 ± 35.91 pA at E12.5, n=16; V_{hold}=+80 mV; $p<0.01$). The increased outward current could suppress subsequent events by repolarizing the membrane potential and by shortening the duration of each event (Spitzer, 2012) which may underlie the disappearance of BaSH-B at E13.5. Acute bath application of 5 mM tetraethylammonium (TEA), which effectively reduces outward current to E12.5-levels (276.76 ± 39.46 pA, n=7; $p<0.01$ *vs.* control), increases event frequency but fails to induce BaSH-B at E13.5 (n=3, data not shown). This suggests that the absence of BaSH-B is not due to increased outward current. To investigate alternative causes of the disappearance of Bash-B at E13.5, we attempted to evoke Bash-B by other means.

A number of neurotransmitter receptor agonists increases event frequency at E13.5 (Hunt *et al.*, 2006*a*), including muscimol ($GABA_A$ agonist), AMPA, and nicotine (nicotinic acetylcholine receptor agonist). In particular, bath application of 100 μM nicotine initially increased frequency of events that propagate along the midline and mimicked Bash-B (n=7), even in the absence of an intact midbrain (n=3). However, events did not propagate in loops, but instead were induced by a rapid firing of the InZ cells, or a group of cells that are more caudal than r2. Also, Bash-B ends consistently after a few minutes. Thus, the mechanism underlying nicotine-induced high frequency firing is probably different from the Bash-B that naturally occurs at E12.5.

Another alternative is that the endogenous Bash-B may fail to occur at E13.5 because events can no longer loop, possibly due to a modification of the looping circuit. To visualize a possible change to the tracks, individual frames of video that show propagation of events were combined into a single image at E12.5 (Fig. 3.7A) or E13.5 (Fig. 3.7B) (see Methods). At E12.5, the resultant image revealed the tracks of event propagation spanning from the midbrain to r2 hindbrain (Fig. 3.7A). A line-intensity scan across the midline shows two peaks separated by 72.4 μm at the isthmus (isth), suggesting that calcium events propagate in two tracks. The two peaks in the line scan are also present in r1 hindbrain (200 μm caudal to the isthmus), where they are farther apart (78.7 μm). The tracks are closer together (64.5 μm) at a position 400 μm caudal to isthmus, and then converge as they get closer to r2, such that they cannot be clearly discerned (r2). The two peaks suggest that the rostral hindbrain has two separate tracks flanking the midline axis at E12.5 (n=4). A line scan across the midbrain shows a wide, single peak (MB, Fig. 3.7A), indicating that the parallel tracks along the midline axis of the hindbrain have converged in the midbrain tegmentum such that the events can cross to the other side of the midline as a single track. Line scan analysis showed that identical tracks are used by events that propagate in loops, or those that are single events (data not shown).

In contrast to E12.5, the line scan analysis yields a single peak at the isthmus and r1 at E13.5 (Fig. 3.7B, n=4). This suggests that E13.5 hindbrain uses a single track instead of two, which may reflect an alteration to the looping circuit itself, preventing propagation in loops. Furthermore, the calcium signal is fainter in the midbrain (Fig. 3.7B), indicating that the extent of propagation is limited in the midbrain tegmentum at

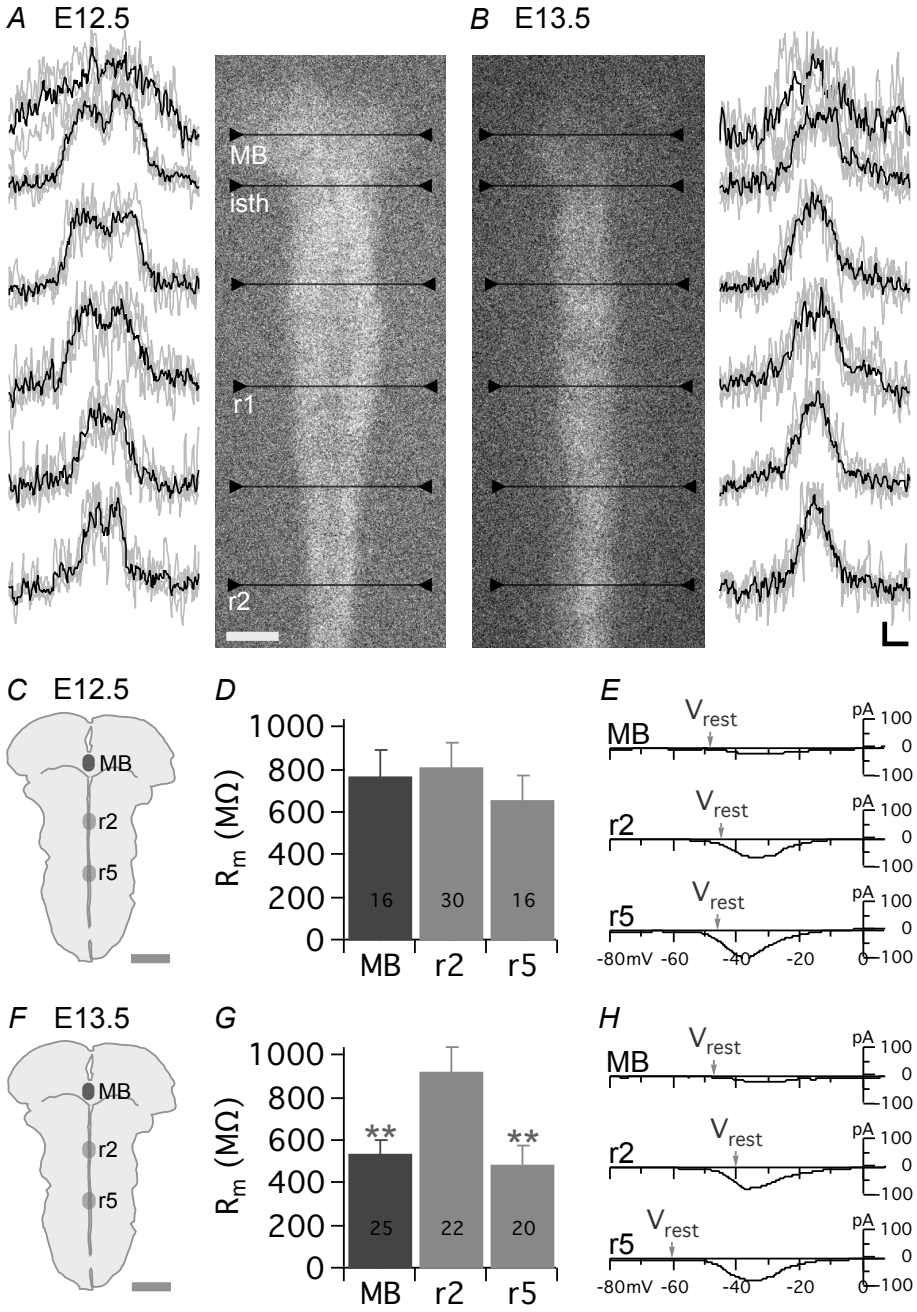

Figure 3.7. Calcium events do not loop at E13.5
A, right: a compiled image of the tracks spanning midbrain tegmentum and r2 hindbrain at E12.5. A, left: the results of the line intensity scans were normalized and superimposed (gray, n=4) along with the averaged line (black). Scale bar: 100 µm (for images in A and B). B, left: a compiled image of the tracks spanning midbrain tegmentum and r2 hindbrain at E13.5. B, right: results of the line intensity scans were normalized and superimposed (gray, n=4) along with the averaged line (black). The positions of the line scans correspond to the lines with inverted arrow heads in the adjacent panel. Scale bar: 0.2 normalized ΔF/F, 50 µm (for line scan plots in A and B). C, positions of the patch clamp recordings at E12.5: midbrain tegmentum 150 µm rostral from isthmus and along midline axis (MB); r2 hindbrain 50 µm rostral to cranial nerve V and along midline axis, closer to one of the two parallel tracks (r2), r5 hindbrain (r5). D, Membrane resistance (MB: n=16; r2: n=30; r5: n=16). E, IV relations showing averaged window current and location of average resting membrane potential (V_{rest}) (arrows) at the three positions. F, positions of the patch clamp recordings at E13.5. G, Membrane resistance (MB: n=25; r2: n=22; r5: n=20). E, IV relations showing averaged window current and location of average resting membrane potential (V_{rest}) (arrows). V_{rest} values are taken from Watari *et al.*, 2012 for r2 and r5. The error bars are SEM. Scale bar: 1 mm (C and F).

E13.5. This may be caused by retraction, which is known to limit the spatial extent of event propagation in r5 hindbrain at E13.5 (Watari *et al.*, 2012). To verify this, we compared passive membrane properties at different stages and positions (Figs. 3.7C-H). At E12.5, before retraction has occurred along the midline of the hindbrain (Watari *et al.*, 2012), membrane resistance in the midbrain and r5 cells is similar (Fig. 3.7D). The resting membrane potential is also not different at these positions, although the mean resting membrane potential in the midbrain (-48.56 ± 2.85 mV, n=16) is more hyperpolarized than the lower voltage range of window current (-44.09 ± 1.47 mV) (Fig. 3.7E). This indicates that retraction has not yet occurred in the midbrain at E12.5. In contrast, at E13.5, midbrain membrane resistance is reduced to the same level as that in r5 (Fig. 3.7G), where we had previously demonstrated that the retraction process of hyperpolarization has already occurred (Watari *et al.*, 2012). This makes the membrane less excitable, possibly hindering propagation of events into and across the midbrain tegmentum. Although midbrain cells do not hyperpolarize, unlike r5 cells (Fig. 3.7H), in both cases the resting membrane potential is outside the range of the window current. Taken together, spatial retraction in the midbrain and convergence of midline tracks in the hindbrain may cause a loss of the looping circuit, and hence prevent Bash-B at E13.5.

Infinite loop? Will it ever end?

Why doesn't looping continue indefinitely? We have observed four independent ways (n=18 episodes in 15 experiments) in which the loops can end: via failures of

propagation; a particular exit pattern in the midbrain; collisions of events; and branching into alternative tracks.

First, looping can end due to a propagation failure, which often occurs spontaneously in the midbrain tegmentum at or near the isthmus (n=7 of 18) (Fig. 3.8A).

The second way the loop ends involves a specific pattern of exit from the midbrain tegmentum (n=6 of 18) (Fig. 3.8B). In some cases, events exit the midbrain back into the hindbrain along both midline tracks simultaneously. When this occurs, events propagate caudally down the hindbrain on both tracks and leave the looping circuit permanently.

Third, the looping event can collide with another event if they are traveling towards each other on the same track (Hughes *et al.*, 2009) and this head-to-head collision causes both events to disappear (n=4 of 18) (Fig. 3.8C). The InZ cells, which fire independently of the looping event, initiate events that propagate rostrally (Fig. 3.8C, red arrows) and collide with the looping event (Fig. 3.8C, black arrow). Not every event from the InZ stops the looping event. A head-to-head collision typically occurs in the midbrain tegmentum, or in the hindbrain where events on two parallel tracks jump across the midline. The collision must be head-to-head otherwise a component of an event may escape into an unoccupied track and continue to propagate along the looping circuit.

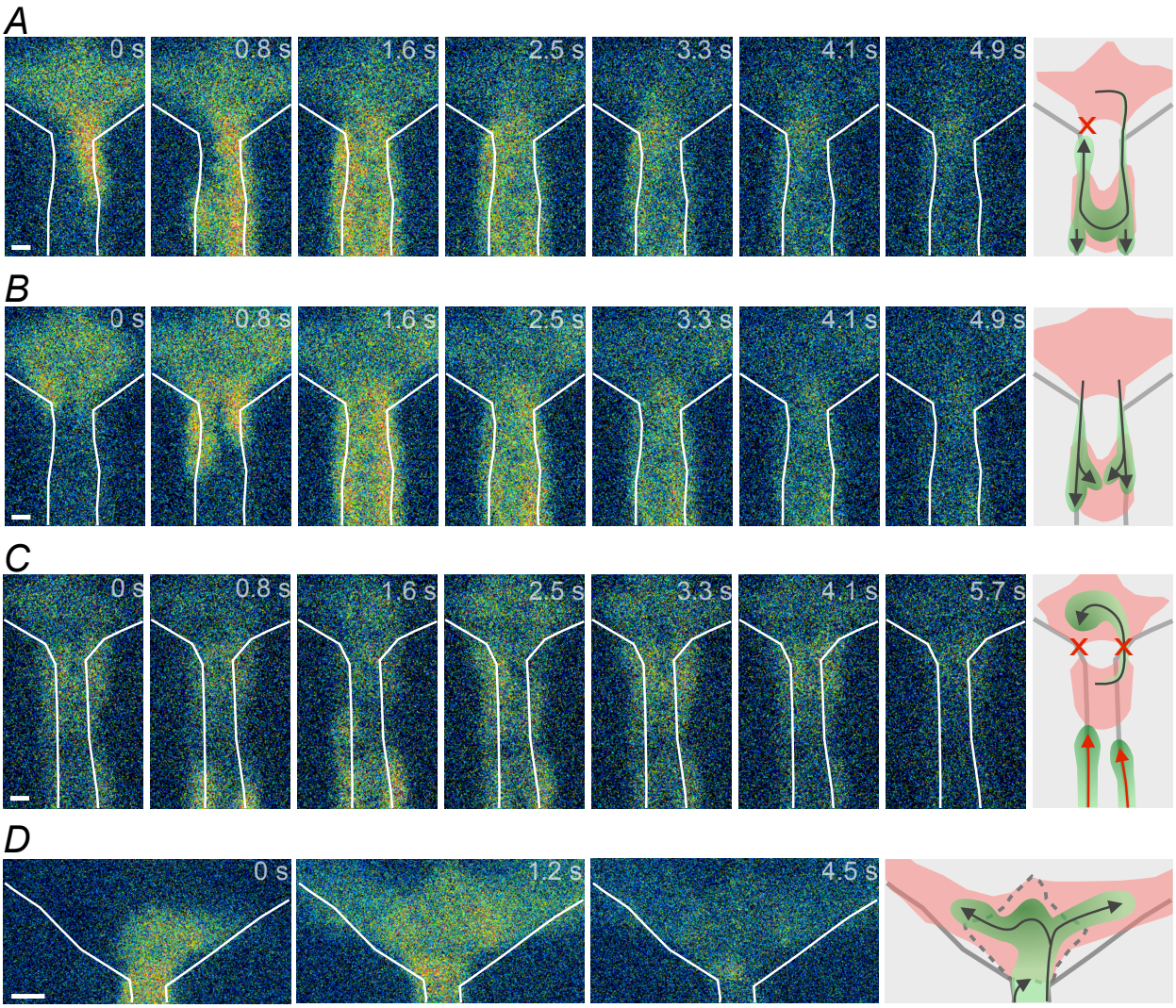

Figure 3.8. Four independent mechanisms that underlie the end of a looping pattern
A, An example of an event in the midbrain-hindbrain loop failing to propagate at or near the isthmus. X indicates the location of propagation failure. B, An example of an event exiting from both sides of the midbrain. C, An example of colliding wavefronts: an event in the midbrain-hindbrain loop (black arrow) collides at the isthmus with an event from the InZ (red arrow) on the left track. The event on the right track arrives at the isthmus slightly later than the left, and it fails to propagate into the midbrain, as described in panel A. X indicates the locations where propagation ends. D, An example of an event propagating dorsolaterally into the midbrain. The area of the midbrain tegmentum through which the event propagated during the loops is outlined with a dotted line. Examples in panels A, B and D were taken from the same brainstem preparation. Scale bars: 50 μm (A, B, C); 100 μm (D).

The fourth way to end Bash-B is sporadic branching of an event out of the looping circuit and into the lateral (dorsal) regions of the midbrain (n=1 of 18) (Fig. 3.8D), as described previously (Rockhill *et al.*, 2009). This sudden branching pushes the event to propagate out of the looping circuit.

Taken together, an episode of Bash-B ends by a variety of methods, and as a result, the duration of Bash-B can vary widely from a few seconds (Fig. 3.1C, middle) to tens of minutes (Fig. 3.1D). The examples in Figures 3.8A, B and D were taken from the same brainstem preparation, demonstrating that the brainstem is capable of ending loops by multiple means.

Looping propagation is inhibited by flupirtine and APV

Inhibitors of spontaneous hindbrain calcium activity such as ketanserin (Hunt *et al.*, 2005) act by preventing initiation and propagation of calcium events, which is a prerequisite for the looping mechanism. Here we looked for a drug that allows initiation of normal midline events but specifically blocks Bash-B. Acute bath application of flupirtine, a known activator of K_v7 channels mediating M current, inhibited Bash-B while sparing the initiation of events at the InZ (n=5 of 5 experiments) (Fig. 3.9A). Events fail to propagate in loops under the influence of flupirtine. However, the target of flupirtine may be something other than K_v7 channels because 20 μM XE-991, an antagonist of the same channel type, has no effect on the occurrence of Bash-B (n=5 of 7 experiments). Because flupirtine can also indirectly inhibit NMDAR, we bath applied APV, and Bash-B was selectively inhibited (n=6 of 7 experiments) (Fig. 3.9B), suggesting that looping requires NMDAR activation. However, activation of this receptor by bath application of 1-10 μM NMDA (n=3) did not induce Bash-B. Thus, the molecular mechanism of Bash-B is not clear. Nevertheless, flupirtine and APV effectively block Bash-B, and these drugs can be used as a tool to further study the role of Bash-B in development.

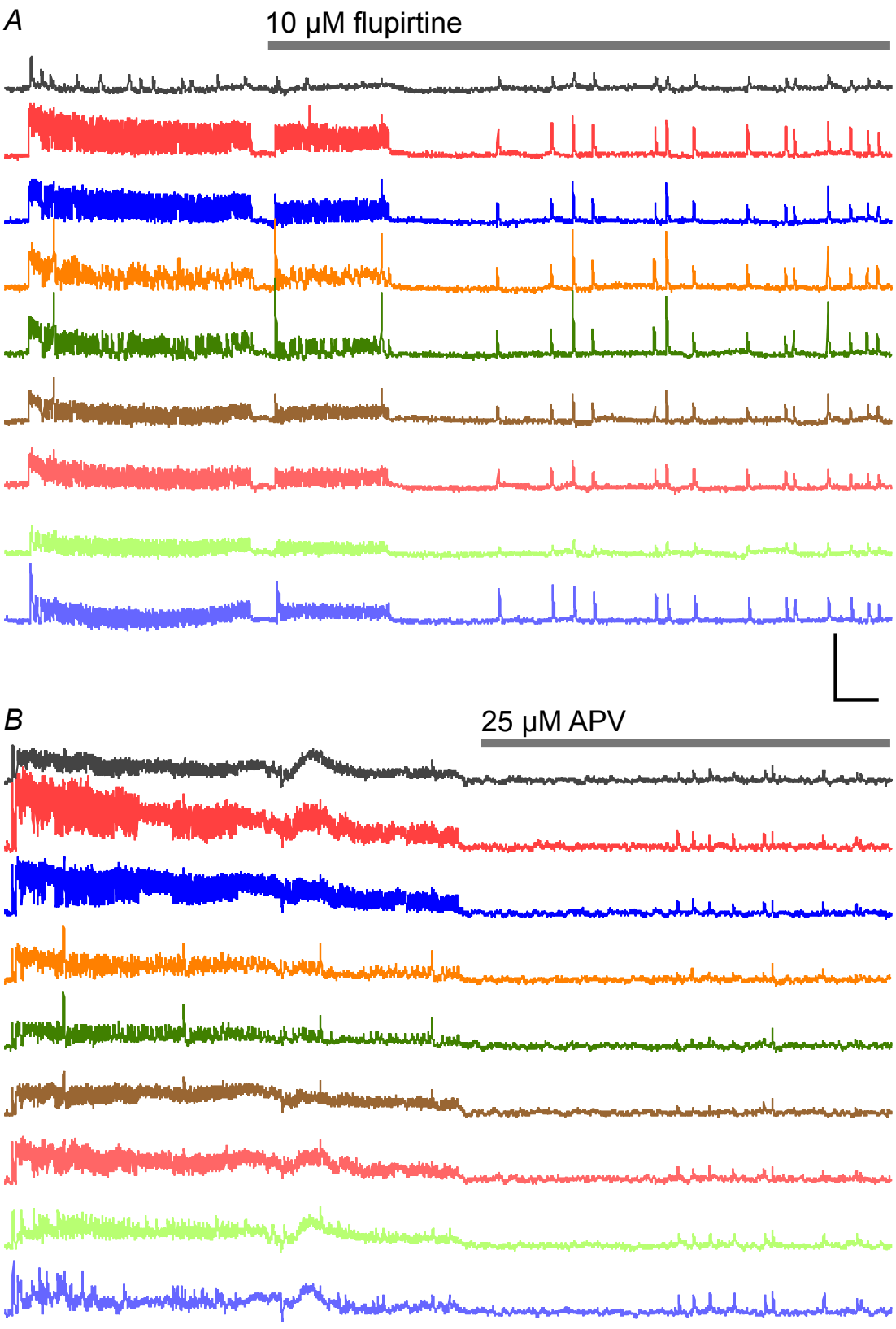

Figure 3.9. Bash-B is selectively inhibited by flupirtine and APV
A, Acute bath application of 10 μM flupirtine inhibits Bash-B (5 of 5 experiments) but not normal midline events. B, Acute bath application of 25 μM APV inhibits Bash-B (6 of 7 experiments). Color of the traces corresponds to location of the ROIs as shown in Figure 3.4. The event amplitudes decrease over time due to photobleaching. Scale bar: 3 ΔF/F and 2 min.

Discussion

A central dogma in neuroscience is that cytoplasmic calcium is maintained at extremely low levels (30-200 nM) at rest and that entry of calcium during electrical activity influences a variety of cellular processes including protein phosphorylation, programmed cell death, and gene expression. The duration of a typical action potential causing calcium entry is on the order of milliseconds. This calcium is cleared within a few seconds (Hille, 2001), making that brief calcium signal a meaningful one. Here, we report the mechanism of a previously uncharacterized phenomenon, Bash-B, where cytoplasmic calcium levels are sustained for an unusually long period of time, up to tens of minutes (Fig. 3.1D). The resulting sustained increase in $[Ca^{2+}]_i$ may impact developmental processes such as proliferation, migration, axonal growth, synaptogenesis, ion channel expression and neurotransmitter specification (Moody and Bosma, 2005; Spitzer, 2012), by influencing gene expression in an activity-dependent manner (Flavell and Greenberg, 2008). Bash-B emerges at E12.5 and disappears within 24 hours, suggesting that Bash-B impacts development in stage- and location-specific manners. The impacted neurons may include raphe serotonergic and ventral tegmental dopaminergic neurons.

A looping circuit is a key underlying mechanism of Bash-B

The key underlying mechanism of Bash-B is a circuit where calcium events propagate in loops involving the midline of midbrain and hindbrain. Although each lap is brief (3-5 s), repetitive laps around this loop effectively extends calcium influx for

minutes at a time. Each lap causes calcium influx at a rate that is faster than the clearance of calcium, resulting in the hallmark above-baseline $[Ca^{2+}]_i$ of Bash-B. The looping mechanism allows cells to experience calcium influx at frequent and regular intervals, influencing processes that require sustained or pulsatile calcium input.

Window current may contribute to spontaneous activity but is not directly causative of loops

Each episode of Bash-B is triggered by an event initiated at the InZ, that then either propagates in loops (Figs. 3.4A-D) or, rarely, is followed by repeated firing from the InZ (without use of the looping circuit [Fig. 3.4C]). In either case, the InZ is essential to triggering Bash-B. Spontaneous firing of InZ cells is supported by decreased resting conductance, depolarized resting membrane potential (Watari *et al.*, 2012), and increased voltage-gated inward current and window current (Fig. 3.5H). High membrane excitability in InZ cells at E12.5 is conducive to Bash-B and a probable cause of the non-looping rapid firing style of Bash-B (Fig. 3.4C). The inward current is predominantly T-type calcium current at earlier stages (Moruzzi *et al.*, 2009), which is postulated to regulate cell proliferation (Capiod, 2011) because the channel shows a range of steady-state voltage where it does not inactivate, creating persistent calcium influx known as “window current” that can be effective even at rest (Bean and McDonough, 1998). Coincidentally, the thickness of the brainstem from ventricular zone to pial surface increases by 120 μm between E11.5 and E12.5 (Rockhill *et al.*, 2009), indicating that cell proliferation correlates with the period when window current increases (Fig. 3.5H).

The coincidence of an increase in window current and the appearance of Bash-B suggest that Bash-B might be a result of persistent membrane depolarization caused by tonic calcium entry. However, current clamp recordings suggest that this is not the case because, during Bash-B, the membrane potential returns to V_{rest} between each depolarization (Fig. 3.5J).

The window current may contribute to, but does not define, the pacemaker in the hindbrain because it is found at rest in cells, such as r5 midline, where initiation does not occur. The r5 midline cells are statistically identical to r2 midline cells in terms of input resistance (Fig. 3.7D), the voltage range of the window current, peak window current, and resting membrane potential (Fig. 3.7E). This implies that other critical factors must be present at r2 midline, a predominant site of initiation, and not at r5; we do not know the factor that defines the pacemaker. Because V_{rest} is within the voltage range of the window current, this steady-state inward current may contribute to cell firing. In support of this, the mean resting membrane potential is positioned within the voltage range of the window current at stages when spontaneous activity is robust (E11.5-E13.5) (Figs. 3.5D-F) whereas it hyperpolarizes below the range at later stages when spontaneous activity ceases (E14.5-E15.5; data not shown) due to retraction (Watari *et al.*, 2012). Therefore, the ability of a midline cell to fire spontaneously may depend on the resting membrane potential relative to the voltage range of the window current.

Refractory period dictates the flow and directionality of calcium waves

The refractory period is proposed to regulate the spread of retinal waves (Butts *et al.*, 1999). In that system, the direction of wave propagation is dependent on the number of recruitable cells, which become refractory for some time after a wave propagates through them. In the hindbrain, when two wavefronts collide (head-to-head collision), propagation of both waves ends (Hughes *et al.*, 2009). Waves cannot back-propagate, dictating a single direction of propagation for each event. Only where propagation is slower, possibly exceeding the refractory period, as in the midbrain tegmentum, can events make U-turns and reverse direction. Therefore, a refractory period likely regulates both directionality and termination of event propagation.

Variants of the looping circuit provide the means to vary frequency of calcium input

The location of the looping circuit designates the inter-peak interval of calcium events to either 3 s (hindbrain-only) or 5 s (midbrain-hindbrain loops). A combination of several properties of the midbrain may explain the slower lap time in midbrain-hindbrain loops: length of the path; delayed propagation at the isthmus; and reduced membrane excitability. First, the path that encompasses the midbrain tegmentum is longer than the track that is restricted to the hindbrain, thus lengthening the single lap time. Second, propagating events appear to “pause” as they reach the isthmus (Rockhill *et al.*, 2009), and the resulting lag may add to the total lap time. Third, midbrain cells have a low density of inward current (Fig. 3.6E) and resting membrane potential hyperpolarized to the voltage range of the window current (Fig. 3.7E); the resultant reduction in membrane excitability may contribute to slower propagation through the midbrain.

These factors, alone or in combination, may work to prolong the time it takes to complete a lap in midbrain-hindbrain loops. The brainstem thus can combine two looping circuits (Fig. 3.4D), each with a unique lap time, to fine tune the total amount of calcium input. The factor that determines the mode of propagation and which looping circuit is utilized is unknown, but a ”barrier” may regulate some events to enter the looping circuit while it forces other events to fail or end propagation.

Midbrain influences the fate of event propagation

A propagating event may enter or exit a looping circuit, change direction, or fail altogether at the midbrain because of two “barriers” regulating propagation in an all-or-none fashion. A probable mechanism of the barriers, one of which is found at the isthmus, and another between the midbrain tegmentum and lateral (dorsal) parts of the midbrain, is incomplete chemical transmission at these borders. Across the latter border, propagation requires activation of a set of neurotransmitter receptors (AChR and GABAR) (Rockhill *et al.*, 2009), suggesting that crossing this border requires chemical transmission. The transmission may still be immature or suboptimal in that propagation fails sporadically, ending the loops. The pause at the isthmus (Rockhill *et al.*, 2009) may be inherent to immature chemical transmission or incomplete track formation because the axon bundles of serotonergic neurons, putative carriers of calcium events on the two parallel tracks along the midline (Fig. 3.7A), are still extending from hindbrain into midbrain tegmentum (Rockhill *et al.*, 2009). The calcium waves propagating across or near these borders during Bash-B may strengthen and fine tune neurotransmission or specify receptor identities.

Neurotransmitter systems that support spontaneous activity changes across stages

Varying calcium inputs during spontaneous activity regulates the neurotransmitter phenotype of a synapse in homeostatic ways (Spitzer, 2012). The amount of calcium input regulates the specification of the serotonin transmitter system in the developing hindbrain of *Xenopus laevis* (Demarque and Spitzer, 2010). Changes in event frequency across stages in the mouse brainstem suggests that neurotransmitter systems could be a target for regulation by spontaneous activity. GABA, which is excitatory in many developing brain structures (Ben-Ari, 2002), increases event frequency at E13.5, but not earlier at E11.5, in the mouse hindbrain (Hunt *et al.*, 2006*a*). Similarly, event frequency is modulated by norepinephrine at E13.5 but not at E11.5. Nicotine can robustly increase event frequency at E13.5 (Hunt *et al.*, 2006*a*), but has no effect at E15.5 (data not shown). The effect of AMPA, and NMDA to a lesser extent, becomes stronger on event frequency by E13.5 compared to E11.5 (Hunt *et al.*, 2006*a*), and this trend progresses to the point that bath application of AMPA induces calcium events in quiescent hindbrain at later stages (Watari *et al.*, 2012). Thus, transmitter systems develop in the embryonic mouse brainstem, possibly mediated by the robust increases in $[Ca^{2+}]_i$ during Bash-B; more work needs to be done to study the impact of Bash-B in transmitter specification.

Bash-B is a novel mechanism by which the participating cells experience calcium influxes at frequent and regular intervals, such that $[Ca^{2+}]_i$ can rise above baseline levels for tens of minutes, a markedly long time for an ion that typically is rigorously maintained at extremely low cytoplasmic levels. This prolonged increase in $[Ca^{2+}]_i$ may

influence cellular processes necessary to the development of participating and neighboring cells, including raphe serotonergic and ventral tegmental dopaminergic neurons.

Acknowledgments

Amanda Tose was a co-author of this work. Special thanks to Bess Navarrete, Veronica Rodriguez, Ashley Lin and Joseph Bosma-Moody for technical assistance, and to Bill Moody for critical reading of the manuscript. Thanks to Horacio de la Iglesia for lending us the 4X objective lens that was crucial to this study. The term, “Bash-B” was originally an acronym for Bart Simpson’s Head-like Butte, and was written, *BaSH-B*. It was named as such because the calcium imaging trace resembled the hairstyle of the cartoon character. Thanks to Lucy Liu and Zeke Barger for suggesting other candidate names. This work is supported by NSF IOS 0952395.

Chapter 4: General Conclusions and Future Directions

Calcium is a unique ion in that it not only acts as a charge carrier that mediates changes in membrane excitability, it also functions as a second messenger. Intracellular calcium regulates many cellular mechanisms including gene expression, which is one of the essential processes during development. This dissertation work describes the regulation of $[Ca^{2+}]_i$ in the developing brainstem at the cellular and molecular level, and identifies two novel mechanisms that modulate $[Ca^{2+}]_i$: the retraction of spontaneous activity, where spatial extent of event propagation changes from being widespread to local (Chapter 2), and the sustained increases in $[Ca^{2+}]_i$ caused by calcium events propagating in looping pathways (Chapter 3).

Each day between E11.5-E15.5, the mouse embryo dramatically increases in size and, in correspondence, the brainstem undergoes robust development every 24 hour period. Patterns of spontaneous activity change across stages, which are tightly regulated spatially. The spatiotemporal extent of calcium event propagation is regulated by changes in passive properties of the membrane, in particular, the resting conductance and resting membrane potential. Generally, calcium events propagate through areas of the brainstem where the resting conductance is relatively low and the resting membrane potential more depolarized. Over time, the spatial extent of the propagation undergoes retraction, and this is caused by a progressive increase in the resting conductance and hyperpolarization of the resting membrane potential. The retraction occurs laterally first, then in the midline cells farthest from the canonical initiation zone (InZ) where most spontaneous activity originates. The last place to undergo retraction is the InZ itself. Between E11.5 and E13.5, the resting potential of

the cells at the InZ is positioned within the voltage range of the inward “window current”, which may contribute to spontaneous activity. The resting membrane potential hyperpolarizes below the voltage range of the window current in the InZ cells after E13.5, and spontaneous activity disappears from the brainstem thereafter. The mechanism of retraction has not been characterized previously in the brainstem or in other parts of the developing nervous system where spontaneous activity occurs. The process of retraction effectively lowers the excitability of the membrane while allowing individual cells to fire. The disappearance of spontaneous activity may be a hint that the hindbrain is switching the mode of cellular communication from global waves of depolarization that sweep across the entire tissue to the adult form of cellular communication, synaptic transmission. It is still unclear as to when the functional synapses form in the embryonic hindbrain. More work needs to be done to understand the timing of synaptogenesis and the role that spontaneous activity plays in it.

Spontaneous activity is most robust between E11.5-E13.5. However, calcium events propagate in distinct patterns at each stage. At E11.5 and E13.5, most events start from a defined baseline. However, at E12.5, episodes of high frequency calcium events, called Bash Bursts (Bash-B) become prevalent. Bash-B is characterized by multiple calcium events occurring at a rate faster than the rate of calcium clearance from the cytoplasm, such that the $[Ca^{2+}]_i$ is sustained above baseline level for a prolonged period of time. In fact, an episode of Bash-B can last tens of minutes, which is an unusually long period of time considering that calcium levels are typically kept at extremely low concentrations in the cytoplasm. The underlying mechanism of Bash-B is a looping circuit, which allows InZ-initiated calcium event to propagate in loops. The

looping circuit is located along the midline of the brainstem, and it can encompass the midbrain and hindbrain or the hindbrain only. The propagation occurring in midbrain-hindbrain loops has a slower lap time compared to hindbrain-only loops, and this effectively differentially regulates the total amount of calcium input at a given time. The looping circuit is a novel mechanism that underlies Bash-B, and it is an effective way for the participating cells to experience calcium inputs at frequent and regular intervals for a prolonged duration of time. The role of Bash-B in development is still unknown. It is possible that the resulting sustained increase in $[Ca^{2+}]_i$ may modulate gene expression, upregulate ion channels, help neurons migrate properly and grow axons to the right target, and possibly even alter the looping circuit to stop Bash-B itself. More work needs to be done to fully understand the downstream effects of Bash-B.

The future goal includes understanding the role of spontaneous activity in neuronal circuit formation and its behavioral outcomes. The spontaneous activity occurs at a time and location when raphe serotonergic and ventral tegmental dopaminergic neurons undergo proliferation, migration and axonal extension within the brainstem, but the role of spontaneous activity in these processes is not known. Appropriate development of both classes of neurons has critical implications for adult behavior, as adults with impaired serotonergic or dopaminergic nervous system are afflicted with neurological disorders such as depression and Parkinson's Disease. Pharmacological agents and or transgenic models that allow manipulation of spontaneous activity will be useful for studying the specific role of that activity in neuronal circuit formation and behavioral outcomes.

References

Aller MI & Wisden W (2008). Changes in expression of some two-pore domain potassium channel genes (KCNK) in selected brain regions of developing mice. *Neuroscience* **151,** 1154–1172.

Bean BP & McDonough SI (1998). Two for T. *Neuron* **20,** 825–828.

Ben-Ari Y (2002). Excitatory actions of gaba during development: the nature of the nurture. *Nat Rev Neurosci* **3,** 728–739.

Bosma MM (2010). Timing and mechanism of a window of spontaneous activity in embryonic mouse hindbrain development. *Ann N Y Acad Sci* **1198,** 182–191.

Butts DA, Feller MB, Shatz CJ & Rokhsar DS (1999). Retinal waves are governed by collective network properties. *J Neurosci* **19,** 3580–3593.

Capiod T (2011). Cell proliferation, calcium influx and calcium channels. *Biochimie* **93,** 2075–2079.

Conhaim J, Easton CR, Becker MI, Barahimi M, Cedarbaum ER, Moore JG, Mather LF, Dabagh S, Minter DJ, Moen SP & Moody WJ (2011). Developmental changes in propagation patterns and transmitter dependence of waves of spontaneous activity in the mouse cerebral cortex. *J Physiol (Lond)* **589,** 2529–2541.

Corlew R, Bosma MM & Moody WJ (2004). Spontaneous, synchronous electrical activity in neonatal mouse cortical neurones. *J Physiol (Lond)* **560,** 377–390.

Crossley PH, Martinez S & Martin GR (1996). Midbrain development induced by FGF8 in the chick embryo. *Nature* **380,** 66–68.

Demarque M & Spitzer NC (2010). Activity-dependent expression of Lmx1b regulates specification of serotonergic neurons modulating swimming behavior. *Neuron* **67,** 321–334.

Fenstermaker AG, Prasad AA, Bechara A, Adolfs Y, Tissir F, Goffinet A, Zou Y & Pasterkamp RJ (2010). Wnt/planar cell polarity signaling controls the anterior-posterior organization of monoaminergic axons in the brainstem. *J Neurosci* **30,** 16053–16064.

Flavell SW & Greenberg ME (2008). Signaling mechanisms linking neuronal activity to gene expression and plasticity of the nervous system. *Annu Rev Neurosci* **31,** 563–590.

Garaschuk O, Hanse E & Konnerth A (1998). Developmental profile and synaptic origin of early network oscillations in the CA1 region of rat neonatal hippocampus. *J Physiol (Lond)* **507 (Pt 1),** 219–236.

Garaschuk O, Linn J, Eilers J & Konnerth A (2000). Large-scale oscillatory calcium waves in the immature cortex. *Nat Neurosci* **3,** 452–459.

Godfrey KB & Swindale NV (2007). Retinal wave behavior through activity-dependent refractory periods. *PLoS Comput Biol* **3,** e245.

Gust J, Wright JJ, Pratt EB & Bosma MM (2003). Development of synchronized activity of cranial motor neurons in the segmented embryonic mouse hindbrain. *J Physiol (Lond)* **550,** 123–133.

Hanson MG, Milner LD & Landmesser LT (2008). Spontaneous rhythmic activity in early chick spinal cord influences distinct motor axon pathfinding decisions. *Brain Res Rev* **57,** 77–85.

Hennig MH, Adams C, Willshaw D & Sernagor E (2009). Early-stage waves in the retinal network emerge close to a critical state transition between local and global functional connectivity. *J Neurosci* **29,** 1077–1086.

Hille B (2001). *Ion Channels of Excitable Membranes (3rd Edition)*, 3rd edn. Sinauer Associates Inc 2001-07-01.

Hughes SM, Easton CR & Bosma MM (2009). Properties and mechanisms of spontaneous activity in the embryonic chick hindbrain. *Dev Neurobiol* **69,** 477–490.

Hunt PN, Gust J, McCabe AK & Bosma MM (2006*a*). Primary role of the serotonergic midline system in synchronized spontaneous activity during development of the embryonic mouse hindbrain. *J Neurobiol* **66,** 1239–1252.

Hunt PN, McCabe AK & Bosma MM (2005). Midline serotonergic neurones contribute to widespread synchronized activity in embryonic mouse hindbrain. *J Physiol (Lond)* **566,** 807–819.

Hunt PN, McCabe AK, Gust J & Bosma MM (2006*b*). Spatial restriction of spontaneous activity towards the rostral primary initiating zone during development of the embryonic mouse hindbrain. *J Neurobiol* **66,** 1225–1238.

Meister M, Wong RO, Baylor DA & Shatz CJ (1991). Synchronous bursts of action potentials in ganglion cells of the developing mammalian retina. *Science* **252,** 939–943.

Momose-Sato Y, Nakamori T & Sato K (2012*a*). Spontaneous depolarization wave in the mouse embryo: origin and large-scale propagation over the CNS identified with voltage-sensitive dye imaging. *Eur J Neurosci* **35,** 1230–1241.

Momose-Sato Y, Nakamori T & Sato K (2012*b*). Pharmacological mechanisms underlying switching from the large-scale depolarization wave to segregated activity in the mouse central nervous system. *Eur J Neurosci* **35,** 1242–1252.

Moody WJ & Bosma MM (2005). Ion channel development, spontaneous activity, and activity-dependent development in nerve and muscle cells. *Physiol Rev* **85,** 883–941.

Mooney R, Penn AA, Gallego R & Shatz CJ (1996). Thalamic relay of spontaneous retinal activity prior to vision. *Neuron* **17,** 863–874.

Moruzzi AM, Abedini NC, Hansen MA, Olson JE & Bosma MM (2009). Differential expression of membrane conductances underlies spontaneous event initiation by rostral midline neurons in the embryonic mouse hindbrain. *J Physiol (Lond)* **587,** 5081–5093.

O'Donovan MJ, Chub N & Wenner P (1998). Mechanisms of spontaneous activity in developing spinal networks. *J Neurobiol* **37,** 131–145.

Rockhill W, Kirkman JL & Bosma MM (2009). Spontaneous activity in the developing mouse midbrain driven by an external pacemaker. *Dev Neurobiol* **69,** 689–704.

Roerig B & Feller MB (2000). Neurotransmitters and gap junctions in developing neural circuits. *Brain Res Brain Res Rev* **32,** 86–114.

Sanders TA, Lumsden A & Ragsdale CW (2002). Arcuate plan of chick midbrain development. *J Neurosci* **22,** 10742–10750.

Shatz CJ (1996). Emergence of order in visual system development. *Proc Natl Acad Sci USA* **93,** 602–608.

Spitzer NC (2006). Electrical activity in early neuronal development. *Nature* **444,** 707–712.

Spitzer NC (2012). Activity-dependent neurotransmitter respecification. *Nat Rev Neurosci* **13,** 94–106.

Wang S, Polo-Parada L & Landmesser LT (2009). Characterization of rhythmic Ca2+ transients in early embryonic chick motoneurons: Ca2+ sources and effects of altered activation of transmitter receptors. *J Neurosci* **29,** 15232–15244.

Watari H, Tose AJ & Bosma MM (2012). Hyperpolarization of resting membrane potential causes retraction of spontaneous Cai2+ transients during mouse embryonic circuit development. *J Physiol (Lond)*; DOI: 10.1113/jphysiol.2012.244954.

Weissman TA, Riquelme PA, Ivic L, Flint AC & Kriegstein AR (2004). Calcium waves propagate through radial glial cells and modulate proliferation in the developing neocortex. *Neuron* **43,** 647–661.

Wong RO (1999). Retinal waves and visual system development. *Annu Rev Neurosci* **22,** 29–47.

VITA

Hirofumi Watari

Education

2013	Ph.D. in Neurobiology & Behavior University of Washington, Seattle, WA
2001	B.S. in Neurobiology *with distinction* B.S. in Biochemistry University of Washington, Seattle, WA

Publications

*Watari H, *Tose AJ, Bosma MM (2013) Looping circuit: a novel mechanism for prolonged spontaneous $[Ca^{2+}]_i$ increases in developing embryonic mouse brainstem. *In preparation*
*These authors contributed equally to this work

Watari H, Tose AJ, Bosma MM (2013) Hyperpolarization of resting membrane potential causes retraction of spontaneous Ca_i^{2+} transients during mouse embryonic circuit development. *J Physiol (Lond)*. 591:973-83

Few, AP, Nanou E, Watari H, Sullivan JM, Scheuer T, Catterall WA (2012) Asynchronous Ca^{2+} current conducted by voltage-gated Ca^{2+} (Ca_V)-2.1 and $Ca_V2.2$ channels and its implications for asynchronous neurotransmitter release. *Proc Natl Acad Sci USA*. 109:E452-60

Pratt KG, Zhu P, Watari H, Cook DG, & Sullivan JM (2011) A novel role for {gamma}-secretase: selective regulation of spontaneous neurotransmitter release from hippocampal neurons. *J Neurosci*. 31:899-906

Jiang X, Lautermilch NJ, Watari H, Westenbroek RE, Scheuer T, Catterall WA (2008) Modulation of $Ca_V2.1$ channels by Ca^{2+}/calmodulin-dependent protein kinase II bound to the C-terminal domain. *Proc Natl Acad Sci USA*. 105:341-6

Watari H, Born DE, Gleason CA (2006) Effects of first trimester binge alcohol exposure on developing white matter in fetal sheep. *Pediatr Res*. 59:560-4

Okamura Y, Nishino A, Murata Y, Nakajo K, Iwasaki H, Ohtsuka Y, Tanaka-Kunishima M, Takahashi N, Hara Y, Yoshida T, Nishida M, Okado H, Watari H, Meinertzhagen IA, Satoh N, Takahashi K, Satou Y, Okada Y, Mori Y (2005) Comprehensive analysis of the ascidian genome reveals novel insights into the molecular evolution of ion channel genes. *Physiol Genomics*. 22:269-82

Abstracts and Presentations at Scientific Meetings

*Watari H, *Tose AJ, Bosma MM (2013) Looping circuit: A novel mechanism for spontaneously raising $[Ca^{2+}]_i$ at rapid and regular intervals in developing embryonic mouse brainstem. *Society for Neuroscience Abstracts*. 29.03
*These authors contributed equally to this work

Watari H, Navarrete EA, Tose AJ, Bosma MM (2012) Precisely timed increase in intracellular calcium regulated by coordinated changes in membrane excitability during development. *Society for Neuroscience Abstracts*. 265.01

Symposium talk, June 1, 2012. Developmental regulation of spontaneous $[Ca^{2+}]_i$ transients. *The Graduate Program in Neurobiology & Behavior Student Symposium*

Watari H, Muir KJ, Bosma MM (2011) Developmental retraction and disappearance of spontaneous synchronous activity may require K channel conductance in embryonic mouse hindbrain. *Society for Neuroscience Abstracts*. 133.08

Caras ML, Pollak J, Fung S, Mehravari A, Watari H (2011) Sustainability of outreach programs over time: A look back through the first five years. *Society for Neuroscience Abstracts*.

Watari H, Muir KJ, Bosma MM (2010) Acute modulation of embryonic mouse hindbrain spontaneous activity by SSRI application. *Society for Neuroscience Abstracts*. 440.14

Georgi S, Smarr B, Corke A, Lee M, Watari H, Caras M, Chudler EH (2010) Expanding Our Reach: Using Technology and the Internet at BAW and in Neuroscience Outreach. *Society for Neuroscience Brain Awareness Week Meeting*.

Pratt KG, Watari H, Cook DG, Sullivan JM (2009) Presenilin 1 modulates spontaneous but not evoked release from hippocampal neurons. *Society for Neuroscience Abstracts*.

Georgi S, Caras M, Harris R, Smarr B, Watari H, White BD, Chudler EH (2008) Expanding our reach: Ideas and resources for neuroscience outreach. *Annual Society for Neuroscience Pacific Northwest Chapter Meeting - University of British Columbia (Vancouver, BC)*.

Smarr B, Georgi S, Harris R, Watari H, White BD, Ting JT, Meitzen J, Wark A, Azevedo T, Barot S, De La Iglesia HO, Chudler EH (2007) Lesson plans for teaching neuroscience to pre-college students. *Society for Neuroscience Abstracts*. 29.10

*White BD, *Watari H, *Ting JT, Sebe JY, Wissman AM, Cherny E, McDevitt RA, Lambert TJ, Meitzen J, Chudler EH (2006) Interactive Brain Awareness Week exhibits offer experience learning: a model for teaching concepts in neuroscience. *Society for Neuroscience Abstracts*. 23.14
*These authors contributed equally to this work

Kelley BG, Ting JT, Watari H, Sullivan JM (2006) Effects of APP overexpression on synaptic transmission of cultured mammalian hippocampal neurons. *Annual Society for Neuroscience Pacific Northwest Chapter Meeting - University of British Columbia (Vancouver, BC)*.

Honors and Awards

Statira Biggs Scholarship (2010)
Society for Neuroscience Next Generation Award (2007)
Learning for Leadership Council Award (2006)

Teaching Experience

2013	Graduate Teaching Assistant Biology 459 - "Developmental Neurobiology"
2005, 2010	Graduate Teaching Assistant Neurobiology 301 - "Introduction to Cellular Neurobiology"

Outreach & Community Service

2012-2013	Foundation for International Understanding Through Students (FIUTS), Facilitator
2011-2013	The Brain Question, Creator and Editor in Chief A world-wide neuroscience outreach project, web application http://students.washington.edu/nbout/TheBrainQuestion/
2009-2012	Disabilities, Opportunities, Internetworking, and Technology (DO-IT) Summer Program, volunteer
2006-2013	Neurobiology & Behavior Community Outreach, Co-founder University of Washington Registered Student Organization
2005-2009	Brain Awareness Week Open House, volunteer and co-organizer
2003-2009	Computer Administrator, volunteer Graduate Program in Neurobiology & Behavior